Journal of Medicinal Chemistry

pubs.acs.org/jmc

Article

Analogues of the Herbicide, *N*-Hydroxy-*N*-isopropyloxamate, Inhibit *Mycobacterium tuberculosis* Ketol-Acid Reductoisomerase and Their Prodrugs Are Promising Anti-TB Drug Leads

Ajit Kandale, Khushboo Patel, Waleed M. Hussein, Shun Jie Wun, Shan Zheng, Lendl Tan, Nicholas P. West, Gerhard Schenk, Luke W. Guddat, and Ross P. McGeary*

Cite This: *J. Med. Chem.* 2021, 64, 1670−1684

Read Online

ACCESS | Metrics & More | Article Recommendations | Supporting Information

ABSTRACT: New drugs to treat tuberculosis (TB) are urgently needed to combat the increase in resistance observed among the current first-line and second-line treatments. Here, we propose ketol-acid reductoisomerase (KARI) as a target for anti-TB drug discovery. Twenty-two analogues of IpOHA, an inhibitor of plant KARI, were evaluated as antimycobacterial agents. The strongest inhibitor of *Mycobacterium tuberculosis* (*Mt*) KARI has a K_i value of 19.7 nM, fivefold more potent than IpOHA (K_i = 97.7 nM). This and four other potent analogues are slow- and tight-binding inhibitors of *Mt*KARI. Three compounds were cocrystallized with *Staphylococcus aureus* KARI and yielded crystals that diffracted to 1.6−2.0 Å resolution. Prodrugs of these compounds possess antimycobacterial activity against H37Rv, a virulent strain of human TB, with the most active compound having an MIC_{90} of 2.32 ± 0.04 μM. This compound demonstrates a very favorable selectivity window and represents a highly promising lead as an anti-TB agent.

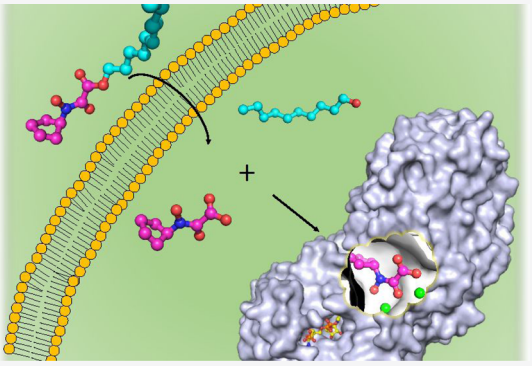

INTRODUCTION

Tuberculosis (TB) is one of the oldest diseases to afflict mankind and remains a major cause of morbidity and mortality, resulting in excess of 1.5 million fatalities each year.[1] It is possible to treat TB using combinations of four first-line drugs, isoniazid, rifampicin, ethambutol, and pyrazinamide, and in severe cases, second-line drugs (e.g., fluoroquinolones, kanamycin, amikacin, and capreomycin) can be included in regimens.[2] However, antimicrobial therapy is prolonged, and patients may suffer from serious side effects, making this collection of chemotherapeutics less than ideal. Increasing occurrences of extensively drug-resistant strains of *Mycobacterium tuberculosis* (*Mt*), the bacteria responsible, and totally drug-resistant TB are also of growing concern.[3] Thus, there is an urgent need to discover new anti-TB drugs, especially those that work by new modes of action.

A potential new target for TB drug discovery is the branched-chain amino acid (BCAA) biosynthesis pathway. This has been suggested because *Mt* is heavily reliant on the endogenous supply of these metabolites and the alveoli have a limited supply of available BCAAs.[4] Across plants, bacteria, and fungi, the biosynthesis of the BCAAs requires seven enzymes to produce leucine, isoleucine, and valine from either two molecules of pyruvate or one molecule of pyruvate and one molecule of 2-ketobutyrate.[5] Ketol-acid reductoisomerase (KARI) (EC 1.1.1.86) is the second enzyme in this pathway. It catalyzes two reactions: an alkyl migration of a methyl or ethyl group (isomerization) followed by an NADPH-mediated reduction of the resulting alpha-keto acid (Scheme 1).[6,7] For the isomerization step, two Mg^{2+} ions and NADPH (or NADH) are required, while the reduction step can be achieved by any of Mg^{2+}, Mn^{2+}, or Co^{2+}, along with NADPH as the preferred hydride donor.[8] The two Mg^{2+} ions and NADPH bind independently to KARI before the binding of the substrate (either (*S*)-2-acetolactate or (*S*)-2-aceto-2-hydroxybutyrate).[9] KARI then converts (*S*)-2-acetolactate to (2*R*)-2,3-dihydroxyisovalerate, leading to the synthesis of valine and leucine. (*S*)-2-Aceto-2-hydroxybutyrate is converted by KARI to (2*R*,3*R*)-2,3-dihydroxy-3-methylvalerate, a precursor of isoleucine.[6,7]

Based on the lengths of their amino acid sequences, KARIs are classified into two categories, a short form (Class-I, ∼340 amino acid residues) found in fungi and most bacteria, for example, *Mt*, and a long form (Class-II, ∼490 amino acid residues) found in plants and some bacteria.[10]

Received: November 5, 2020
Published: January 29, 2021

https://dx.doi.org/10.1021/acs.jmedchem.0c01919
J. Med. Chem. 2021, 64, 1670−1684

Scheme 1. Alkyl Migration and Reduction Reactions Catalyzed by KARI, and Structures of Experimental Herbicides, IpOHA, and Hoe 704, Which are Known to Inhibit Plant KARIs

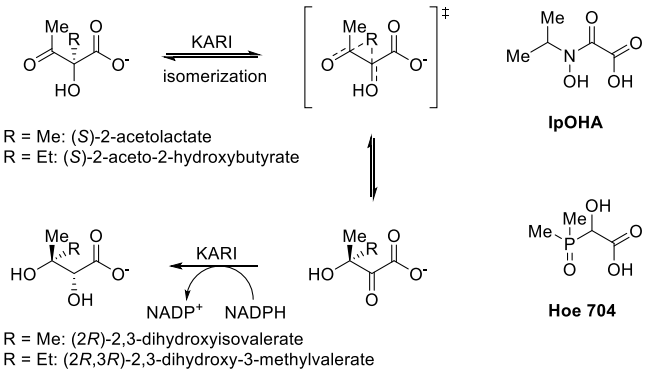

Since the BCAAs are synthesized by plants, fungi, and bacteria but not by mammals, inhibitors of the first enzyme of this pathway, acetohydroxyacid synthase (AHAS), have proven to be effective herbicides and fungicides with low toxicity,[11,12] and two studies[4,13] have shown that AHAS inhibitors can prevent the growth of *Mt* in infected mice. Thus, inhibition of other enzymes from the BCAA pathway may also be an effective strategy to develop novel biocides. Compounds such as *N*-hydroxy-*N*-isopropyloxamate (IpOHA) and 2-dimethylphosphinoyl-2-hydroxyacetic acid (Hoe 704) (Scheme 1) are potent substrate analogue inhibitors of plant KARI.[14] IpOHA only weakly inhibits the growth of three *Mt* strains at concentrations in the range 60−1000 μM.[4] In contrast, IpOHA potently inhibits *Escherichia coli* KARI by slow- and tight-binding with an initial K_i of 160 nM, decreasing to 22 pM (final steady-state K_i).[14]

Previously, we have reported that IpOHA has a K_i value of 97.7 nM for *Mt*KARI[15] and thus represents an excellent starting point for anti-TB drug discovery. Here, we report the syntheses of twenty-two IpOHA analogues, their inhibition of *Mt*KARI, and the structure determination of three of the most potent inhibitors in complex with *Staphylococcus aureus* (*Sa*) KARI, an enzyme which is 56% identical and 76% homologous to *Mt*KARI.[16,17] Prodrugs of these compounds were also tested against avirulent (H37Ra) and virulent (H37Rv) strains of *Mt*.

RESULTS AND DISCUSSION

Inhibitor Design. Initially, a series of IpOHA analogues (22 analogues, Table 1) was designed and evaluated by the docking of trial compounds into the active site of *Slackia exigua* (*Se*) KARI.[18] The structure of *Sa*KARI was not available at the time, and the structure of *Mt*KARI[16] was not considered suitable since the cofactor, NADPH, is not visible. However, the active site residues of *Se*KARI are identical to those of *Mt*KARI, and its structure was solved in the presence of IpOHA and NADPH and so was considered to be a better structure for use in docking calculations. The chemical structures and docking scores (DSs) of the trial compounds are shown in Table 1. The DS of **5b** is −7.8, which matches the DS of IpOHA. Compounds **4d**, **5a**, **5c**, **5d**, and **5e** also have excellent DSs ranging from −5 to −8. Since the binding poses and interactions of all docked molecules are similar to those observed for the *Se*KARI·Mg^{2+}·NADPH·IpOHA complex,

Table 1. K_i Values of the Synthesized Compounds for *Mt*KARI and DSs with *Se*KARI[a]

Compound	Structure	K_i (nM)	Docking score
4a	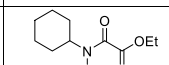	1020 ± 160	-1.4
4b	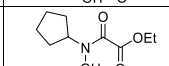	32.2 ± 1.6	-2.1
4c	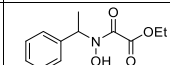	152.2 ± 14.6	(*R*) -4.2* (*S*) -3.9*
4d	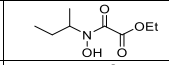	44.7 ± 3.4	(*R*) -5.2 (*S*) -5.5
4e	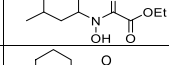	2660 ± 190	(*R*) -2.4 (*S*) -3.0
5a	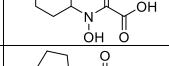	39.6 ± 3.3	-5.1
5b	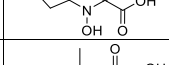	19.7 ± 1.4	-7.8
5c	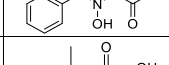	97.7 ± 8.3	(*R*) -7.8* (*S*) -7.7*
5d	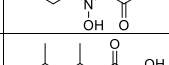	22.6 ± 1.6	(*R*) -8.1 (*S*) -7.6
5e	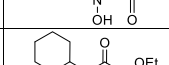	660 ± 90	(*R*) -6.8 (*S*) -7.0
7a	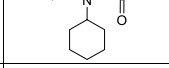	>20000	ND
7b	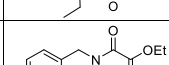	>20000	-3.2
7c	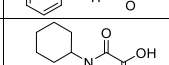	>20000	ND
8a	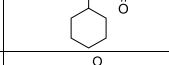	>20000	ND
8b	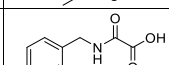	>20000	-3.7
8c	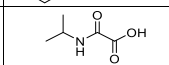	>20000	-4.5
8d	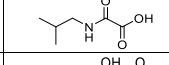	>20000	-5.8
8e	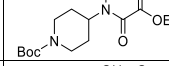	>20000	-6.1
11	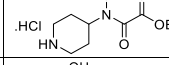	>20000	ND
12	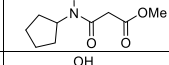	3080 ± 190	-3.3
13	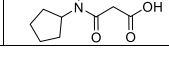	>20000	-1.7
14	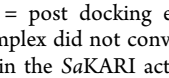	>20000	-5.0

[a]Note: ND = post docking energy minimization of the enzyme−inhibitor complex did not converge. *Scores obtained by docking the compounds in the *Sa*KARI active site (see below).

https://dx.doi.org/10.1021/acs.jmedchem.0c01919
J. Med. Chem. 2021, 64, 1670−1684

Scheme 2. Synthesis of IpOHA Analogues 5a−e[a]

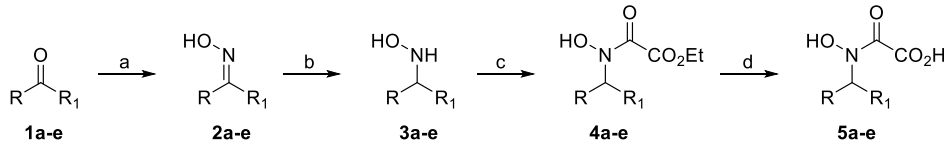

[a]Reagents and conditions: (a) $NH_2OH{\cdot}HCl$, NaOH, EtOH, H_2O, 60 °C, 3 h; (b) $NaCNBH_3$, 4 M HCl-dioxane, MeOH, rt, 3 h; (c) $ClCOCO_2Et$, DIPEA, THF, 4 °C, 3 h; and (d) KOH, THF, H_2O, Δ, 1 h.

there is a strong suggestion that these compounds would also inhibit *Mt*KARI.

Chemistry. The designed compounds were synthesized by coupling hydroxylamines or amines with ethyl oxalyl chloride (EOC) in the presence of *N*,*N*-diisopropylethylamine (DIPEA) (Schemes 2−4). Hydrolysis using aqueous KOH to cleave the ester side chains, in all cases, gave the corresponding carboxylic acid derivatives. The hydroxylamines (**3a−e**) needed for the synthesis of **5a−e** were prepared by the reaction of the respective ketones (**1a−e**) with hydroxylamine hydrochloride to obtain oximes (**2a−e**), followed by reduction to the corresponding *N*-alkylhydroxylamines (**3a−e**) using $NaCNBH_3$.

The amines **6a−e** required for the syntheses of **8a−e** were purchased from Sigma-Aldrich. Amides **8a−e** were prepared as shown in Scheme 3. Coupling of amines **6a−e** with EOC with either pyridine or DIPEA as a base gave the ethyl esters (**7a−e**) which were then saponified using aqueous KOH.[19] Finally, the piperidine-hydroxamate **12**[20] and the *β*-carboxyhydroxamate **14** were synthesized as shown in Scheme 4.

Scheme 3. Synthesis of Oxamic Acids 8a−e[a]

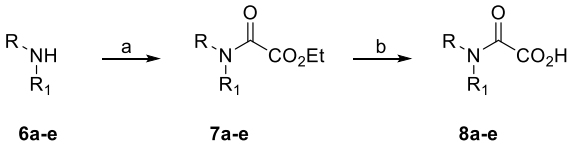

[a]Reagents and conditions: (a) $ClCOCO_2Et$, DIPEA or pyridine, THF or CH_2Cl_2 and (d) KOH, THF, H_2O.

Scheme 4. Synthesis of Piperidine-hydroxamate, 12, and *β*-carboxyhydroxamate, 14[a]

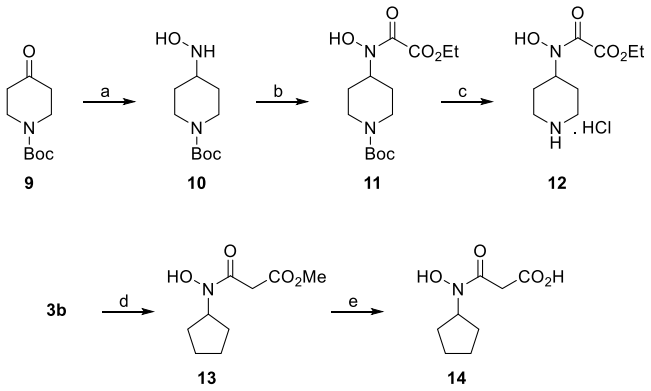

[a]Reagents and conditions: (a) (i) $NH_2OH{\cdot}HCl$, NaOAc, AcOH (ii) $NaCNBH_3$, MeOH, rt, 16 h; (b) $ClCOCO_2Et$, DIPEA, THF, 3 h; (c) 4 M HCl-dioxane, THF, rt, 1 h; (d) $ClCOCH_2CO_2Me$, DIPEA, THF, 4 °C, 3 h; and (e) KOH, THF, H_2O, Δ, 1 h.

Inhibition Studies. An initial study was performed to assess whether the IpOHA analogues exhibit time-dependent binding to *Mt*KARI by monitoring the progress of the interaction over 1 h (exemplified for **5b** in Figure 1A). Based on the observed slow binding, all subsequent assays were performed by first incubating the assay mixture (*Mt*KARI, NADPH, Mg^{2+}, and IpOHA) for 30 min. The reaction was then initiated by adding (*S*)-2-acetolactate (longer incubation times did not affect the magnitude of the determined K_i values). In the first round of screening, the inhibitory effects of the analogues were tested at a concentration of 100 *μ*M; **4a−e** and **5a−e** were identified as strong inhibitors of *Mt*KARI. In contrast, the compounds devoid of an *N*-hydroxyl group (**7a−c** and **8a−e**) are very weak inhibitors (Table 1). Compound **11** bearing a Boc-protected piperidine has negligible inhibition. This is attributed to the large size of this protecting group preventing it from entering the active site. Upon removal of the Boc-protecting group (**12**), inhibition was observed, supporting this hypothesis. The malonate derivatives **13** and **14** exhibited poor inhibition compared to their homologues **4b** and **5b**, showing the importance of the *α*-ketoacid moiety for activity.

Determination of K_i Values. K_i values were determined by fitting inhibition data to either the Morrison equation (for tight-binding inhibitors **4b−d**, **5a**, and **5b−d**) or the standard inhibition equation (for weaker inhibitors **4a**, **4e**, **5e**, and **12**) against *Mt*KARI[21] (Table 1). Compound **5b** showed a fivefold increase in potency (K_i of 19.7 ± 1.4 nM) compared to IpOHA (K_i = 97.7 ± 8.3 nM)[15] and is the most active in the series (Figure 1).

Compounds **4b**, **4d**, **5a**, **5b**, and **5d** are more potent than IpOHA against *Mt*KARI. **5b** is the most potent with an approximately fivefold decrease in K_i compared to IpOHA. The ethyl ester analogue (**4b**) of **5b** has a K_i of 32.2 nM. It is possible that **4b** might undergo ester hydrolysis under assay conditions, thus converting it to its corresponding carboxylic acid derivative (**5b**), which may be the main contributor to the observed inhibition of *Mt*KARI. To investigate this hypothesis, the compounds present in the assay mixture were monitored by mass spectrometry. If the ethyl ester group of **4b** was being hydrolyzed to the corresponding carboxylic acid in the assay, the presence of **5b** with a mass of 172.06 amu for the M−H ion in the negative mode was expected. However, we only observed a peak at 224.10 amu, corresponding to the $[M + Na]^+$ ion of the starting ester **4b**. This confirmed that the ester was stable under the assay conditions for 30 min of incubation and the enzyme inhibition obtained was solely due to **4b** itself.

https://dx.doi.org/10.1021/acs.jmedchem.0c01919
J. Med. Chem. 2021, 64, 1670−1684

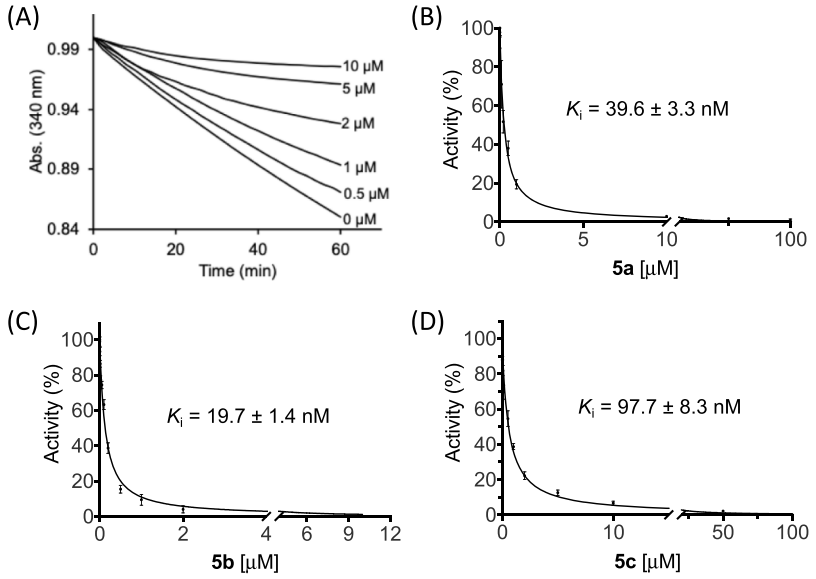

Figure 1. Inhibition of *Mt*KARI by IpOHA analogues (**5a**–**c**). (A) Progress curves illustrating time-dependent inhibition of *Mt*KARI by **5b**. (B–D) Inhibition plots for **5a**, **5b**, and **5c**, respectively, fitted to the Morrison equation.[22]

Table 2. Data Collection and Refinement Statistics for *Sa*KARI in Complex with Mg^{2+}, NADPH, and 5a–c[a]

	5a	5b	5c
Data Collection			
unit cell length (Å)	a = 65.72, b = 79.03, c = 69.64	a = 64.48, b = 80.39, c = 67.30	a = 65.82, b = 78.91, c = 69.37
unit cell angle (deg)	$\alpha = \gamma$ = 90, β = 101.39	$\alpha = \gamma$ = 90, β = 90.13	$\alpha = \gamma$ = 90, β = 101.10
space group	$P2_1$	$P2_1$	$P2_1$
unique reflections [$I > 0\sigma(I)$]	41,023 (2928)	79,180 (3915)	56,182 (3161)
total observations [$I > 0\sigma(I)$]	140,268 (9792)	595,692 (27,606)	193,605 (10,382)
completeness (%)	98.9 (90.9)	99.8 (97.0)	98.8 (87.4)
R_{merge}	0.070 (0.519)	0.081 (0.740)	0.063 (0.476)
R_{pim}	0.052 (0.388)	0.034 (0.322)	0.045 (0.345)
$\langle I\rangle/\langle\sigma(I)\rangle$	8.7 (1.6)	13.2 (1.9)	9.1 (1.7)
subunits per asymmetric unit	2	2	2
Refinement			
resolution range (Å)	43.61–2.09	46.63–1.67	43.50–1.88
R_{work}	0.170 (0.197)	0.154 (0.157)	0.162 (0.165)
R_{free}	0.209 (0.234)	0.192 (0.196)	0.207 (0.209)
average B-factor (Å^2)	33.08	20.31	30.23
RMS Deviation from Ideal			
bond length (Å)	0.003	0.010	0.017
bond angle (deg)	0.564	1.185	1.474
Ramachandran Plot Statistics			
favored	97.84%	97.53%	96.89%
outliers	0%	0%	0%
residues not visible in density	1 and 328–334 in both subunits	1 and 328–334 in both subunits	1 and 323–334 (chain A), 1 and 328–334 (chain B)

[a]Values in parentheses are for the outer resolution shell. $R_{merge} = \sum_{hkl}\sum_i |I_i(hkl) - (I(hkl))| / \sum_{hkl}\sum_i I_i(hkl)$. $R_{pim} = \sum_{hkl}\left[\frac{1}{[N(hkl)-1]}\right]^{1/2}\sum_i |I_i(hkl) - (I(hkl))| / \sum_{hkl}\sum_i I_i(hkl)$ where $I_i(hkl)$ is the observed intensity and $I(hkl)$ is the average intensity obtained from multiple observations of symmetry-related reflections.

The strong binding of compounds **5a**–**e** to *Mt*KARI is likely due to the presence of an α-carboxyhydroxamate group that can bind to the two Mg^{2+} ions and also the type of substituents on the nitrogen atom which fits inside the hydrophobic pocket of the active site. Compounds with smaller alicyclic rings or aliphatic chains, as seen in **5b** and **5d**, showed maximum inhibition. Increasing the ring size to cyclohexane (**5a**) or the length of the aliphatic side chain (4-methyl-2-pentyl substitution in **5e**) attached to the nitrogen atom led to a decrease in activity. Replacing the aliphatic functionality on the nitrogen atom with an aromatic moiety (2-phenylethyl in **5c**) also lowered the activity compared to **5b**.

***Sa*KARI Inhibition Assays.** Attempts to crystallize these compounds in complex with *Mt*KARI were unsuccessful. Hence, we chose *Sa*KARI for these experiments. The active site residues in *Sa*KARI and *Mt*KARI are highly conserved (Supporting Information, Figure S1). To also confirm the functional similarity of these two enzymes, the inhibitors **5a**–**c**

https://dx.doi.org/10.1021/acs.jmedchem.0c01919
J. Med. Chem. 2021, 64, 1670–1684

were shown also to be potent inhibitors of *Sa*KARI. The K_i value of **5b** is twofold lower for *Sa*KARI than for *Mt*KARI (8.5 ± 1.0 nM vs 19.7 ± 1.4 nM), while for **5c**, the K_i value is twofold higher for *Sa*KARI than for *Mt*KARI (193 ± 8.4 nM vs 97.7 ± 8.3 nM). However, the K_i of **5a** for *Sa*KARI is ∼25-fold higher (1.0 ± 0.4 μM) compared to *Mt*KARI (39.6 nM), a difference that may be due to the presence of isoleucine instead of valine in position 248 of *Sa*KARI (Supporting Information, Figure S1), reducing the size of the active site binding pocket.

Crystal Structures of *Sa*KARI in Complex with 5a−c. The diffraction data for the *Sa*KARI·Mg^{2+}·NADPH in complex with **5a**, **5b**, and **5c** were collected to be 2.09, 1.67, and 1.88 Å, respectively. The data collection and refinement statistics are shown in Table 2. In the asymmetric unit, a dimer of *Sa*KARI is present with the two active sites at the interface of the two subunits. The electron density of the polypeptide is continuous from the N- to C-termini apart from the first N-terminal residue and last seven C-terminal residues of each subunit. The overall fold of the dimer is similar (rmsd: 0.15−0.54 Å) to that of the *Sa*KARI·Mg^{2+}·NADPH·IpOHA complex.[17]

The electron density maps after fitting **5a**, **5b**, and **5c** with full occupancy showed negative density where the *N*-hydroxy group is located and additional spherical positive density nearby (Figure 2). This suggests that the N−O bonds in a

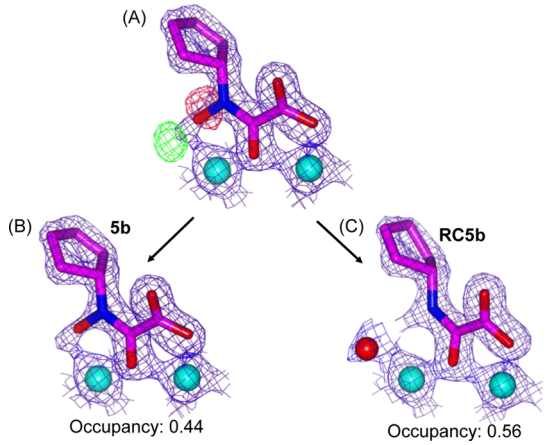

Figure 2. Electron density maps for **5b** in the SaKARI. Mg^{2+}.NADPH.**5b** complex. (A) $2F_o-F_c$ (blue: 2σ) and difference maps (red: -3σ and green: 3σ) after fitting **5b** at 100% occupancy. (B,C) $2F_o-F_c$ map after fitting **5b** and **RC5b** at an occupancy of 0.44 and 0.56, respectively (PDB code: 6C5N). Cyan spheres represent the Mg^{2+} ions, and the red sphere represents water.

fraction of these inhibitors were cleaved to amide products. Re-refinements using combinations of intact (**5a**, **5b**, or **5c**) and deoxy forms (**RC5a**, **RC5b**, or **RC5c**) of the inhibitors with variable occupancies confirmed that both were present in the active site. Figure 2 shows **5b** as an example. When **RC5b** is bound, a water molecule is present to complete the coordination sphere of Mg^{2+}. This water molecule and the hydroxyl oxygen of the intact compound (**5b**) would be only 1.7 Å apart, so their simultaneous existence in the active site is implausible. A high-resolution mass spectrum of the sample of **5b** used for crystallization was obtained to confirm its purity, and no peaks corresponding to the deoxy form were observed. Therefore, the reduction must have occurred during crystallization. These observations are in accordance with our previous results obtained for the crystal structure of the *Sa*KARI·Mg^{2+}·NADPH·IpOHA complex which also showed the presence of the reduced form of IpOHA.[17]

The electron density maps showed that the nicotinamide ring of NADPH is puckered (and likely reduced) when in complex with **5b** and **5c** and planar (and likely oxidized) when in complex with **5a** (Figures 3A and 4B). When the intact

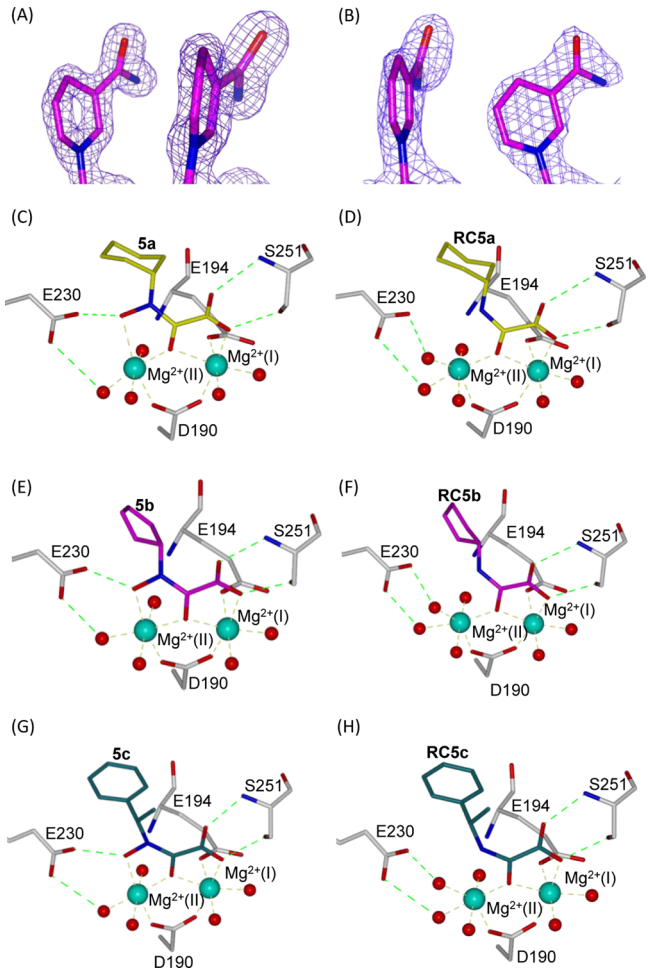

Figure 3. active site of *Sa*KARI in complex with Mg^{2+}, NADPH, and the IpOHA analogues. (A) $2F_o-F_c$ electron density map for nicotinamide of NADPH in complex with **5b** contoured at 2σ. (B) $2F_o-F_c$ electron density map for nicotinamide of NADPH in complex with **5a** contoured at 2σ. (C) **5a** and (D) its deoxy form **RC5a** shown as yellow sticks. (E) **5b** and (F) its deoxy form **RC5b** are shown as pink sticks. (G) **5c** and (H) its deoxy form **RC5c** shown as dark green sticks (PDB codes: **5a** 6C55, **5b** 6C5N, and **5c** 6BUL). The metals and water molecules are shown as cyan and red spheres, respectively, and active site residues are shown as white sticks. The metal ligand bonds are shown in yellow, and hydrogen bonds are shown in green.

inhibitors are bound in the active site, the N−OH group interacts with Mg^{2+}(II), resulting in a near perfect octahedral geometry. The hydroxyl oxygen is ∼2.4 Å from the carboxylate oxygen of E230, suggesting a hydrogen bond, with either E230 or the hydroxyl being the proton donor (Figure 3C,E,G). When the hydroxyl group is cleaved from these inhibitors, an additional water molecule is observed. This does not superimpose with the hydroxyl but fills a nearby space where it also forms a hydrogen bond with E230. This difference results in a distortion of the octahedral geometry at the Mg^{2+}(II) site. Irrespective of whether the intact or cleaved

https://dx.doi.org/10.1021/acs.jmedchem.0c01919
J. Med. Chem. 2021, 64, 1670−1684

inhibitor is present in the crystal structures, the Mg^{2+}(I) site is unaltered with the positions of the six ligands conserved in an octahedral arrangement (Figure 3). The carboxyl groups of each inhibitor make important interactions, with one of the oxygen atoms forming a hydrogen bond with the amide of S251 and the other oxygen atom ligating the Mg^{2+}(I) (Figure 3). The cyclohexane ring in **5a** has a chair conformation, whereas the cyclopentane ring in **5b** adapts a half-chair conformation.

The rings of **5a**, **5b**, and **5c** make hydrophobic interactions with the surrounding residues P132, L198, I234, and I250 (Figure 4). In the first conformation of **5c**, its methyl group forms a hydrophobic interaction with the side chain of A254 (Figure 4C). The active site pockets in Figure 4A,C are expanded by ∼1−2 Å compared to those in Figure 4B,D. The cyclohexane ring of **5a** and the positioning of the methyl group of **5c** require more space in the active site. The orientation of the methyl group in the second conformation of **5c** results in the phenyl ring moving deeper into the pocket, leading to a contraction of the active site (Figure 4D).

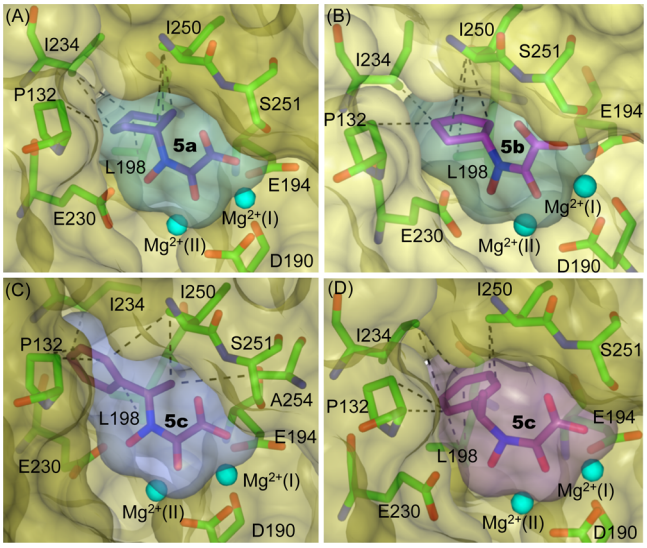

Figure 4. Hydrophobic interactions for **5a**−**5c** at the active site. The active site residues are shown as green sticks, and the compounds are shown in different shades of purple sticks. The hydrophobic interactions are shown as black dashed lines. Metals are shown as cyan spheres.

The binding of **5a**−**c** to *Sa*KARI causes rotation of the N-terminal domains of the dimer (Figure 5A). In addition, there is a movement of the helix (P132−E142) by 1.72 Å. Binding of **5a** and **5c** in the conformation shown in Figure 4C perturbs the position of P132, E230, and I234 (Figure 5B). This confirms that the active site is flexible. In contrast, S251 and D190 remain in the same position in all structures. The potencies of these compounds correlate with the degree to which the active site is contracted. The most potent inhibitor **5b** (K_i = 8.5 nM for *Sa*KARI) binds in a way that the active site is contracted, and the binding of the least potent **5a** (K_i = 1 μM) keeps the active site comparatively expanded. The activity of **5c** (K_i = 193 nM) is intermediate between **5a** and **5b**, consistent with the observation that there are two alternative conformations in the active site (Figure 4C,D).

Comparison of the Molecular Docking Results with the Crystal Structures. Since we determined the crystal structures of **5a**−**c** in complex with *Sa*KARI·Mg^{2+}·NADPH, we were able to compare these experimental data with results predicted from in silico docking. The predicted docking orientations of **5a** and **5b** were consistent with the crystal structures (Figure 6). The cyclohexane ring in **5a** is in a chair conformation in both experimental and docked structures. The confirmation of **5b** in the crystal structure matches well with the pose predicted from the docking, other than a slight rotational offset of the cyclopentane ring away from S251- (Figure 6B). However, the lengths of the metal−oxygen coordination bonds predicted by docking were shorter (by 0.1−0.3 Å) than those observed in the crystal structures.

When either the *R* or *S* enantiomer of **5c** was docked into the active site of *Se*KARI, the software could not predict any

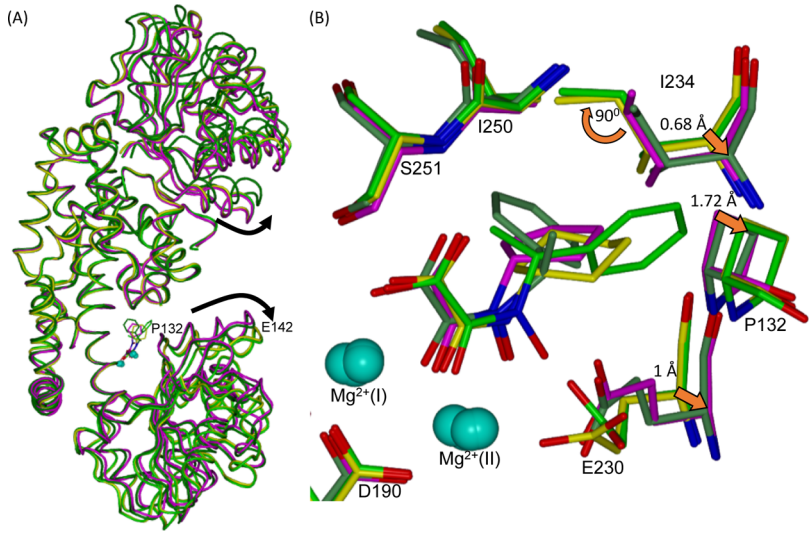

Figure 5. Comparison of the overall fold and active site of the *Sa*KARI in complex with the newly synthesized inhibitors. **5a** (yellow), **5b** (magenta), conformation 1 of **5c** (light green), and conformation 2 of **5c** (dark green) (PDB codes: **5a** 6C5S, **5b** 6C5N, and **5c** 6BUL). Metals are shown as cyan spheres. (A) Black arrows indicate rotation of the domain associated with the active site and substrate binding. (B) Orange arrows indicate movement of amino acids in the active site.

https://dx.doi.org/10.1021/acs.jmedchem.0c01919
J. Med. Chem. 2021, 64, 1670−1684

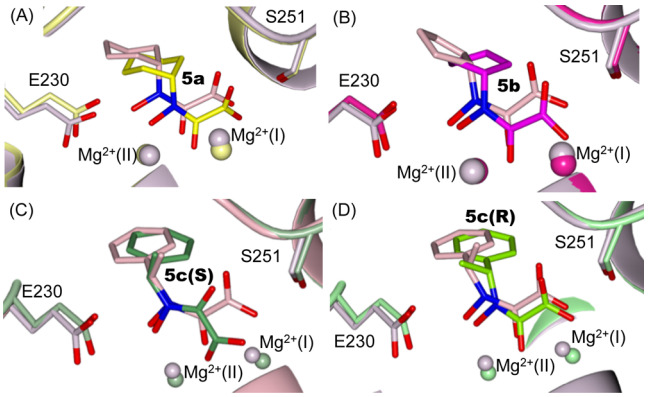

Figure 6. Comparison of the docking and crystal structure results. The crystal structures of all the compounds are shown in light pink. The docked structure for **5a** is in yellow, **5b** is in magenta, and **5c** is in light green for the *R* isomer and dark green for the *S* isomer. **5a** and **5b** were docked using the *Se*KARI·Mg^{2+}·NADPH·IpOHA complex. The **5c** enantiomers were docked using the *Sa*KARI·Mg^{2+}·NADPH·IpOHA complex.

valid poses due to failure in postdocking energy minimization. This could be due to insufficient space in the *Se*KARI active site. However, our experimental data show that **5c** has K_i values of 97.7 nM for *Mt*KARI and 193 nM for *Sa*KARI, confirming its potent inhibition. Thus, to investigate further, the docking of both enantiomers of **5c** into the *Sa*KARI·Mg^{2+}·NADPH·**5c** structure was performed (Figure 6). Scores of −7.8 and −7.7 for the *R* and *S* isomers, respectively, were obtained, suggesting that these isomers could have similar potencies. However, the prediction made by Glide showed that the mode of binding of the *S* isomer was different to that observed in the crystal structure. Instead of the carbonyl oxygen of (*S*)-**5c** bridging the metal ions as seen in the crystal structure, a carboxylate oxygen performs this role in the docked structure (Figure 6C). The predicted docking of the *R* isomer of **5c** shows a binding mode similar to that observed in the crystal structure of the *Sa*KARI·Mg^{2+}·NADPH·**5c** complex (i.e., the carbonyl oxygen bridges the metal ions, Figure 6D). The fact that the crystal structure of *Sa*KARI with **5c** has only the *S* isomer bound suggests that it favors the *S* isomer. Thus, the true K_i value of the *S*-enantiomer of **5c** may be less than the 97.7 nM obtained for the racemate.

Antimycobacterial Activity of *Mt*KARI Inhibitors. Although several of the 22 IpOHA analogues are potent inhibitors of *Mt*KARI, none exhibited MIC_{90} values <200 μM (data not shown). Figure 7A shows, as an example, the inhibition of H37Rv growth due to compound **5b**. A likely reason for their lack of activity is that their hydrophilicity prevented them from crossing the complex membrane of *Mt*. To investigate this possibility, prodrugs were synthesized by esterifying the carboxylate group of the most potent inhibitor,

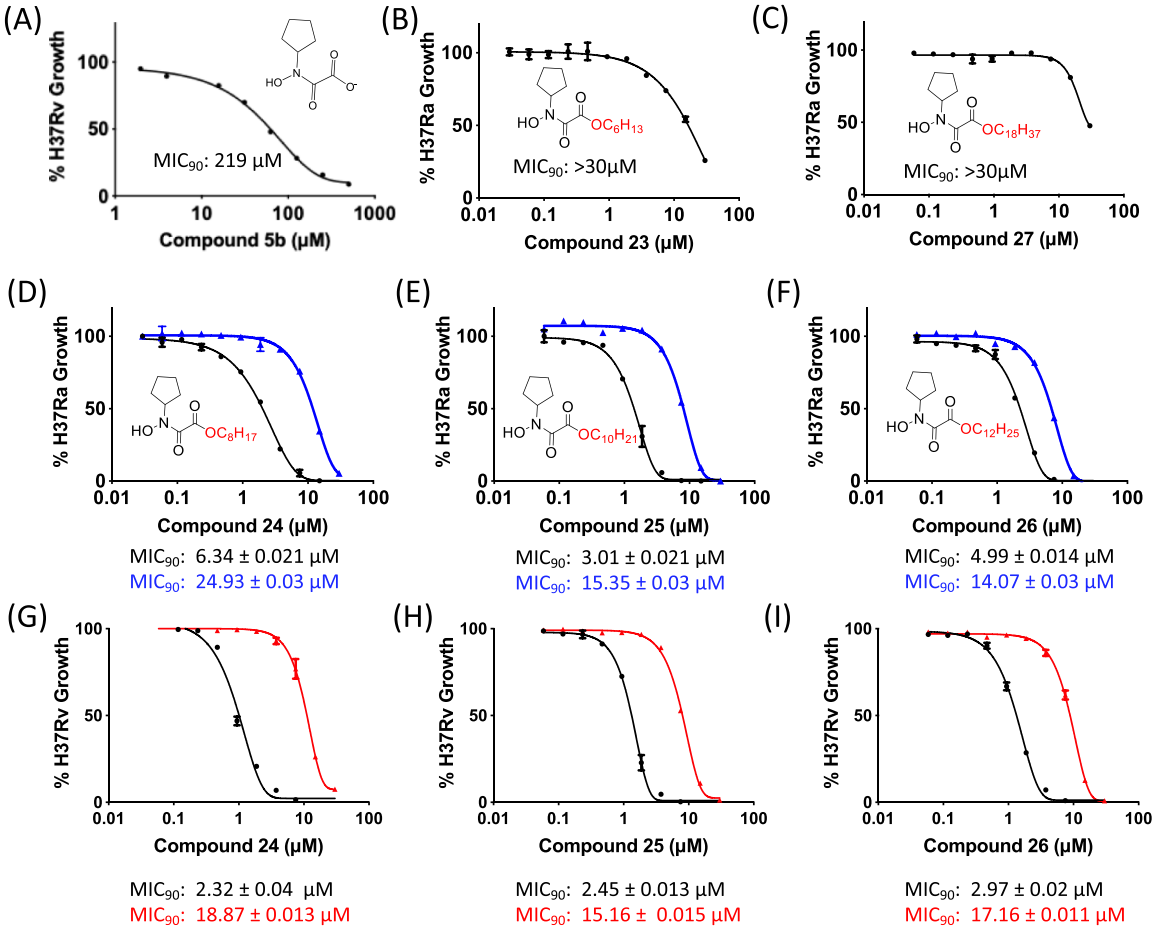

Figure 7. Antimycobacterial activity of the prodrugs of **5b**. (A) Inhibition of H37Rv growth by **5b**. (B–F) Inhibition of H37Ra growth by **23**–**27** in the absence (black) and in the presence (blue) of BCAAs. (G–I) Inhibition of H37Rv growth by **24**–**26** in the absence (black) and in the presence (red) of BCAAs.

https://dx.doi.org/10.1021/acs.jmedchem.0c01919
J. Med. Chem. 2021, 64, 1670−1684

Scheme 5. Synthesis of Esters 23−27[a]

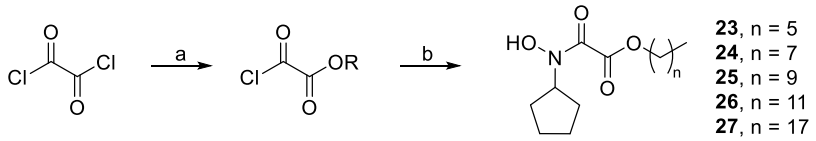

[a]Reagents and conditions: (a) ROH, CH_2Cl_2, 0 °C, 14 h and (b) **5b**, DIPEA, THF, 0 °C, 14 h.

5b, adding long-chain lipophilic structures of various lengths, giving derivatives **23−27** (Scheme 5). Prodrugs derived from **5b**, esterified with octanol (**24**), decanol (**25**), and dodecanol (**26**), exhibited excellent MIC_{90} values in the range of 3−6 μM for H37Ra and 2−3 μM for H37Rv strains (Figure 7D−I), while derivatives **23** and **27** (Figure 7 B,C), derived from hexanol and octadecanol, respectively, showed lower activity with MIC_{90} values >30 μM. To confirm that the antimycobacterial activity of these compounds was not due to the prodrug attachments themselves, the long-chain alcohols were all tested in *Mt* assays (Supporting Information, Figure S3). All these have MIC_{90} values >30 μM. Thus, it appears that these prodrugs can cross the membrane of *Mt* and then be hydrolyzed by cellular esterases to release the KARI inhibitor (**5b**).

To confirm that the target of the active compounds is the BCAA pathway, the assays were repeated but with media supplemented with 1 mM each of leucine, isoleucine, and valine, concentrations much higher than expected in vivo (typical concentrations in the alveoli range from 100 to 200 μM[23]). After the addition of the BCAAs, the activities of the compounds were reduced by three- to ninefold, confirming the BCAA pathway as their target (Figure 7D−I). Furthermore, **24−26** have very similar MIC_{90} values against H37Rv, regardless of which ester group was attached (Figure 7G−I). Interestingly, the reduction in the inhibitory activity of **24−26** in H37Rv (six- to ninefold) upon the addition of the BCAAs was more pronounced than that observed in H37Ra (three- to ninefold).

Cytotoxicity of Compound 25 in Mammalian Cell Lines. To access cytotoxicity, the most potent prodrug, **25**, was assessed using an MTT assay in three mammalian cell lines (RAW 264.7, HEK 293, and SW620). The compound was not toxic up to 50 μM concentration, which is about 16-fold higher than the MIC_{90} in H37Rv cells (Figure 8).

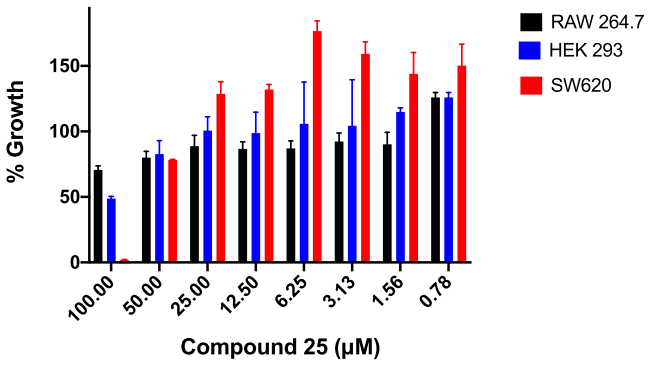

Figure 8. MTT assay of **25** against three mammalian cell lines. RAW 264.7 cells are viable up to 100 μM, and HEK293 and SW620 cells are viable up to 50 μM concentration of the compound.

CONCLUSIONS

Twenty-two analogues of IpOHA were designed, synthesized, and assayed against *Mt*KARI. The K_i values of these compounds were as low as 19 nM (**5b**). Cell susceptibility assays showed that the parent compounds were inactive but lipophilic prodrugs of **5b** successfully inhibited the growth of *Mt* with MIC_{90} values as low as 2.3 μM. Supplementation of the growth media with BCAAs demonstrated that the target was the BCAA pathway. Moreover, the prodrugs were still effective against *Mt* even at high BCAA concentrations. Crystal structures of several IpOHA analogues (**5a−c**) in complex with *Sa*KARI·Mg^{2+}·NADPH demonstrated a conserved mechanism of inhibitor binding, resulting in closure of the active site (Figures 4 and 5). This is the first comprehensive study that demonstrates that a designed KARI inhibitor is a promising drug lead to combat TB.

EXPERIMENTAL SECTION

Materials. All reagents and solvents required for the synthesis were purchased from Sigma-Aldrich, Merck, Novachem, Chembridge chemicals, and AK scientific. Silica gel (0.040−0.063 mm) for flash chromatography was purchased from Merck. *Mt*KARI[16] and *Sa*KARI[17,24] were expressed and purified as described previously. NADPH was purchased from Sigma-Aldrich. (*S*)-2-Acetolactate was synthesized by alkaline hydrolysis of the methyl ester of 2-hydroxy-2-methyl-3-oxobutyrate purchased from Sigma-Aldrich. Although a racemic mixture is obtained as a result of hydrolysis, only (*S*)-2-acetolactate is a substrate for KARI. The concentration of the (*S*)-isomer was determined by measuring the consumption of NADPH at 340 nm until all of the (*S*)-2-acetolactate was depleted. Small aliquots were stored at −80 °C until use. Purity of synthesized compounds is >95%, as determined by elemental analyses and ^{1}H NMR spectroscopy.

Chemical Synthesis. *Synthesis of Oximes **2a−e**.* Hydroxylamine hydrochloride (0.074 mol, 5.13 g) and sodium hydroxide (0.148 mol, 5.92 g) were dissolved in a sufficient distilled water and ethanol mixture (3:1) in a 500 mL round bottom flask. The ketone **1a−e** (0.05 mol) was added to this solution. More ethanol was added if necessary to solubilize the ketone completely. The mixture was heated at 60 °C. The reaction was monitored by thin-layer chromatography (TLC) and continued until complete disappearance of the initial ketone (approximately 3 h). After the reaction, the ethanol was evaporated under reduced pressure and the aqueous layer was extracted with CH_2Cl_2 (3 × 30 mL). The combined organic layers were washed with water, dried over anhydrous sodium sulfate, filtered, and evaporated under reduced pressure to give the crude oxime. The product was recrystallized from petroleum ether and dichloromethane (DCM) (9:1).

*Cyclohexanone Oxime (**2a**).* From 0.05 mol (4.9 g) of cyclohexanone (**1a**) in ethanol−water (20 and 60 mL), a light brown solid was obtained (1.82 g, 32%); mp 86−88 °C (lit.[25] mp 87−89 °C); TLC (R_f = 0.80, petroleum ether and ethyl acetate, 9:1).

*Cyclopentanone Oxime (**2b**).* From 0.05 mol (4.2 g) of cyclopentanone (**1b**) in ethanol−water (20 and 60 mL), a light brown solid was obtained (2.2 g, 45%); mp 57−58 °C (lit.[26] mp 57−58.5 °C); TLC (R_f = 0.74, petroleum ether and ethyl acetate, 8:2).

*Acetophenone Oxime (**2c**).* From 0.25 mol (30 g) of acetophenone (**1c**) in ethanol−water (100 and 300 mL), a light

https://dx.doi.org/10.1021/acs.jmedchem.0c01919
J. Med. Chem. 2021, 64, 1670−1684

brown solid was obtained (30.4 g, 90%); mp 59−60 °C (lit.[27] mp 59−60 °C); TLC (R_f = 0.88, petroleum ether and ethyl acetate, 7:3).

*2-Butanone Oxime (**2d**).* From 0.25 mol (18 g) of 2-butanone (**1d**) in ethanol−water (100 and 300 mL), a yellow liquid was obtained (11.3 g, 52%); bp 151−153 °C (lit.[27] bp 152 °C); TLC (R_f = 0.48, petroleum ether and ethyl acetate, 7:3).

*4-Methylpentan-2-one Oxime (**2e**).* From 0.25 mol (25 g) of 4-methylpentan-2-one (**1e**) in ethanol−water (100 and 300 mL), a pink solid was obtained (19.5 g, 68%); mp 61.5−63 °C (lit.[28] mp 63 °C); TLC (R_f = 0.64, petroleum ether and ethyl acetate, 8:2).

*Reduction of Oximes **2a−e** to Hydroxylamines **3a−e**.* Reductions were carried out according to the reported procedure.[29] To a methanolic solution of oxime (**2a−e**) (2 mmol), sodium cyanoborohydride (4 mmol, 0.252 g) and approximately 10 mg of a bromocresol green indicator were added, followed by the dropwise addition of 4 M dioxane-HCl under a nitrogen atmosphere to maintain the yellow color (pH 4) for 30 min. The reaction mixture was stirred at room temperature for 3 h. The precipitated salt was filtered off, and the filtrate was evaporated under reduced pressure. The residue was taken up in 200 mL of water, and 6 M potassium hydroxide solution was added until alkaline (pH 12). The aqueous layer was saturated with sodium chloride and extracted with CH_2Cl_2 (3 × 30 mL). The combined organic extracts were washed with brine, dried over anhydrous sodium sulfate, and filtered. The filtrate was evaporated under reduced pressure to obtain the hydroxylamine.

*N-Cyclohexylhydroxylamine (**3a**).* From 0.02 mol (2.3 g) of cyclohexanone oxime (**2a**) in 50 mL of methanol, a colorless solid was obtained (2.1 g, 89%); mp 139−140 °C (lit.[30] mp 138−140 °C); TLC (R_f = 0.16, chloroform and methanol, 9:1).

*N-Cyclopentylhydroxylamine (**3b**).* From 0.02 mol (2.0 g) of cyclopentanone oxime (**2b**) in 50 mL of methanol, a colorless solid was obtained (1.12 g, 56%); mp 91.5−92.5 °C (lit.[31] mp 92−93 °C); TLC (R_f = 0.49, chloroform and methanol, 9:1).

*N-(1-Phenylethyl)hydroxylamine (**3c**).* From 0.02 mol (2.7 g) of acetophenone oxime (**2c**) in 20 mL of methanol, a colorless solid was obtained (0.90 g, 33%); mp 69−71 °C (lit.[32] mp 69−71 °C); TLC (R_f = 0.38, petroleum ether and ethyl acetate, 7:3).

*N-(But-2-yl)hydroxylamine (**3d**).* From 0.04 mol (3.5 g) of 2-butanone oxime (**2d**) in 40 mL of methanol, a colorless solid was obtained (1.96 g, 55%); mp 96−97.5 °C (lit.[30] mp 97 °C); TLC (R_f = 0.37, petroleum ether and ethyl acetate, 1:1).

*N-(4-Methylpentan-2-yl)hydroxylamine (**3e**).* From 0.04 mol (4.6 g) of 4-methylpentan-2-one oxime (**2e**) in 40 mL of methanol, a yellow solid was obtained (2.88 g, 62%); mp 52−53.5 °C (lit.[28] mp 63 °C); TLC (R_f = 0.24, petroleum ether and ethyl acetate, 8:2). ^{1}H NMR (300 MHz, $CDCl_3$, 25 °C): δ 5.52 (bs, 2H, N**H**O**H**), 2.99−3.10 (m, 1H, CH_3C**H**NH), 1.59−1.72 (m, 1H, CH_3C**H**CH_3), 1.13−1.43 (m, 2H, CHC**H**$_2$CH), 1.08−1.10 (d, 3H, J = 6.0 Hz, C**H**$_3$CHNH), 0.89−0.89 (d, 6H, J = 6.0 Hz, C**H**$_3$CHC**H**$_3$); ^{13}C NMR (75 MHz, $CDCl_3$, 25 °C): δ 55.3 (CH_3**C**HNH), 43.0 (CH**C**H$_2$CH), 24.9 (CH_3**C**HCH_3), 23.2 (**C**H$_3$CHCH_3), 22.4 (CH_3CH**C**H$_3$), 18.0 (**C**H$_3$CHNH).

*Synthesis of Hydroxamates **4a−e** and Amides **7a−b**.* To a solution of hydroxylamines (**3a−e**) or amines (**6a−c**) (1−10 mmol) in 20 mL of anhydrous tetrahydrofuran (THF) was added DIPEA (2 equiv). To this solution, EOC (1.1 equiv) was added dropwise at 4 °C during 15 min under an atmosphere of nitrogen. After the addition, the ice bath was removed, the reaction mixture was allowed to warm to the room temperature, and stirring was continued for 3 h. The precipitated salt was filtered off, and the filtrate was evaporated under reduced pressure to get the crude ester, which was purified by flash chromatography, eluting with petroleum ether and ethyl acetate (7:3).

*Ethyl N-Cyclohexyl-N-hydroxyoxamate (**4a**).* From 0.005 mol (0.58 g) of *N*-cyclohexylhydroxylamine (**3a**) in 20 mL of anhydrous THF, a yellowish orange solid was obtained (1.02 g, 94%); mp 81.3−82.1 °C (lit.[33] mp 82 °C); TLC (R_f = 0.80, petroleum ether and ethyl acetate 1:1); ^{1}H NMR (300 MHz, $CDCl_3$, 25 °C): δ 4.37 (q, 2H, CH_3C**H**$_2$, J = 7.3 Hz), 4.03−4.07 (m, 1H, C_5H_{10}C**H**−**N**), 1.10−1.89 (m, 10H, C_5**H**$_{10}$CH−N), 1.6 (t, 3H, CH_2C**H**$_3$, J = 7.3 Hz); ^{13}C NMR (75 MHz, $CDCl_3$, 25 °C): δ 163.7 (**C**OO), 160.3 (**C**ON), 62.4 (**C**H$_2$CH$_3$), 55.3 (C_5H_{10}**C**H), 28.5, 25.2, 24.8, 13.9; HRMS (ESI/micrOTOF-Q) m/z: $[M + Na]^+$ calcd for $C_{10}H_{17}NO_4Na$, 238.1050; found, 238.1048; Anal. Calcd for $C_{10}H_{17}NO_4$: C, 55.80; H, 7.96; N, 6.51. Found: C, 55.76; H, 8.00; N, 6.49.

*Ethyl N-Cyclopentyl-N-hydroxyoxamate (**4b**).* From 0.01 mol (1.01 g) of *N*-cyclopentylhydroxylamine (**3b**) in 20 mL of anhydrous THF, a brown solid was obtained (830 mg, 41%); mp 47.0−49.2 °C; TLC (R_f = 0.38, petroleum ether and ethyl acetate, 9:1); ^{1}H NMR (300 MHz, $CDCl_3$, 25 °C): δ 8.00 (bs, 1H, N−O**H**), 4.67−4.79 (m, 1H, C_4H_8C**H**−**N**), 4.36 (q, 2H, CH_3C**H**$_2$, J = 7.3), 1.41−2.03 (m, 8H, C_4**H**$_8$CH−N), 1.34−1.38 (t, 3H, C**H**$_3$CH$_2$, J = 7.3 Hz); ^{13}C NMR (75 MHz, $CDCl_3$, 25 °C): δ 163.5 (**C**OO), 160.3 (**C**ON), 62.5 (**C**H$_2$CH$_3$), 56.6 (C_4H_8**C**H), 29.4, 28.2, 25.0, 24.7, 13.9; HRMS (ESI/micrOTOF-Q) m/z: $[M + Na]^+$ calcd for $C_9H_{15}NO_4Na$, 224.0893; found, 224.0890; Anal. Calcd for $C_9H_{15}NO_4$: C, 53.72; H, 7.51; N, 6.96. Found: C, 53.58; H, 7.45; N, 6.94.

*Ethyl N-(1-Phenylethyl)-N-hydroxyoxamate (**4c**).* From 0.003 mol (0.41 g) of *N*-(1-phenylethyl)hydroxylamine (**3c**) in 20 mL of anhydrous THF, a colorless solid was obtained (250 mg, 35%); mp 77.6−78.8 °C (lit.[33] mp 78 °C); TLC (R_f = 0.42, petroleum ether and ethyl acetate, 7:3); ^{1}H NMR (300 MHz, $CDCl_3$, 25 °C): δ 7.29−7.43 (m, 5H, C_6**H**$_5$), 6.92 (bs, 1H, N−O**H**), 5.69 (q, 1H, J = 6.0, C**H**CH_3), 4.39 (q, 2H, CH_3C**H**$_2$, J = 7.0 Hz), 1.65 (d, 3H, CHC**H**$_3$, J = 6.0), 1.39 (t, 3H, C**H**$_3$CH$_2$, J = 7.0); ^{13}C NMR (75 MHz, $CDCl_3$, 25 °C): δ 162.8 (**C**OO), 160.3 (**C**ON), 138.2, 128.7, 127.6, 126.9, 62.4 (**C**H$_2$CH$_3$), 54.3 (**C**HCH$_3$), 15.6, 13.9; HRMS (ESI/micrOTOF-Q) m/z: $[M + Na]^+$ calcd for $C_{12}H_{15}NO_4Na$, 260.0893; found, 260.0894: $[M + H]^+$ calcd for $C_{12}H_{16}NO_4$, 238.1074; found, 238.1079; Anal. Calcd for $C_{12}H_{15}NO_4$: C, 60.75; H, 6.37; N, 5.90. Found: C, 60.56; H, 6.36; N, 5.90.

*Ethyl N-Isobutyl-N-hydroxyoxamate (**4d**).* From 0.005 mol (0.45 g) of *N*-(isobutyl)hydroxylamine (**3d**) in 20 mL of anhydrous THF, an orange liquid was obtained (580 mg, 59%); TLC (R_f = 0.75, petroleum ether and ethyl acetate, 1:1); ^{1}H NMR (300 MHz, $CDCl_3$, 25 °C): δ 4.35 (q, 2H, CH_3C**H**$_2$, J = 7.0 Hz), 4.18−4.29 (m, 1H, CH_3CH_2C**H**CH_3), 1.49−1.60 (m, 2H, CH_3C**H**$_2$CHCH$_3$), 1.18−1.41 (m, 6H, C**H**$_3$CH$_2$CHC**H**$_3$), 0.93 (t, 3H, C**H**$_3$CH$_2$, J = 7.0); ^{13}C NMR (75 MHz, $CDCl_3$, 25 °C): δ 169.8 (**C**OO), 163.5 (**C**ON), 62.9 (**C**H$_2$CH$_3$), 53.5 (CH_3CH_2**C**HCH_3), 25.9, 16.7, 13.9, 10.6; HRMS (ESI/micrOTOF-Q) m/z: $[M + Na]^+$ calcd for $C_8H_{15}NO_4Na$, 212.0893; found, 212.0898: $[M + H]^+$ calcd for $C_8H_{16}NO_4$, 190.1074; found, 190.1077; Anal. Calcd for $C_8H_{15}NO_4$: C, 50.78; H, 7.99; N, 7.40. Found: C, 50.77; H, 7.84; N, 7.07.

*Ethyl N-(4-Methyl-pent-2-yl)-N-hydroxyoxamate (**4e**).* From 0.01 mol (1.17 g) of *N*-(4-methyl-pent-2-yl)hydroxylamine (**3e**) in 20 mL of anhydrous THF, a yellow liquid was obtained (1.45 g, 66%); TLC (R_f = 0.61, petroleum ether and ethyl acetate, 6:4); ^{1}H NMR (300 MHz, $CDCl_3$, 25 °C): δ 4.53−4.60, m, 1H, $(CH_3)_2$CHCH$_2$C**H**CH$_3$, 4.37, q, 2H, CH_3C**H**$_2$, J = 7.0 Hz, 1.80−1.89, m, 1H, $(CH_3)_2$C**H**CH$_2$CHCH$_3$, 1.33−1.70, m, 6H, $(CH_3)_2$CHCH$_2$CHC**H**$_3$ and C**H**$_3$CH$_2$, 1.24, dd, 2H, J = 6.0, 6.0, $(CH_3)_2$CHC**H**$_2$CHCH$_3$, 0.86−0.97, m, 6H, $(CH_3)_2$CH; ^{13}C NMR (75 MHz, $CDCl_3$, 25 °C): δ 164.3 (**C**OO), 160.4 (**C**ON), 62.5 (**C**H$_2$CH$_3$), 50.0 (N−**C**HCH$_3$), 41.7 ($(CH_3)_2$C**H**CH$_2$), 24.9 ($(CH_3)_2$**C**HCH$_2$CHCH$_3$), 22.8 and 22.2 ($(CH_3)_2$CHCH$_2$CHC**H**$_3$), 17.3 ($(CH_3)_2$CHCH$_2$C**H**CH$_3$), 13.9 (**C**H$_3$CH$_2$); HRMS (ESI/micrOTOF-Q) m/z: $[M + Na]^+$ calcd for $C_{10}H_{19}NO_4Na$, 240.1206; found, 240.1209: $[M + H]^+$ calcd for $C_{10}H_{20}NO_4$, 218.1387; found, 218.1391; Anal. Calcd for $C_{10}H_{19}NO_4$: C, 55.28; H, 8.81; N, 6.45. Found: C, 55.18; H, 8.51; N, 6.07.

*Ethyl N,N-Dicyclohexyloxamate (**7a**).* From 0.01 mol (1.81 g) of dicyclohexylamine (**6a**) in 20 mL of anhydrous THF, a colorless solid was obtained (1.46 g, 52%); mp 88.9−90.1 °C; TLC (R_f = 0.94, petroleum ether and ethyl acetate, 1:1); ^{1}H NMR (300 MHz, $CDCl_3$, 25 °C): δ 4.32, q, 2H, CH_3C**H**$_2$, J = 7.3 Hz, 2.98−3.21, m, 2H, 2(C_5H_{10}C**H**), 1.02−2.47, m, 20H, 2(C_5**H**$_{10}$CH), 1.35, t, 3H, C**H**$_3$CH$_2$, J = 7.3; ^{13}C NMR (75 MHz, $CDCl_3$, 25 °C): δ 163.6 (**C**OO), 161.9 (**C**ON), 61.4 (**C**H$_2$CH$_3$), 59.2 (C_5H_{10}**C**H), 55.7 (C_5H_{10}**C**H), 31.0, 29.4, 26.4, 25.7, 25.1, 25.0, 14.0 (CH_3); HRMS (ESI/micrOTOF-Q) m/z: $[M + Na]^+$ calcd for $C_{16}H_{27}NO_3Na$, 304.1883; found, 304.1878: $[M + H]^+$ calcd for $C_{16}H_{28}NO_3$,

https://dx.doi.org/10.1021/acs.jmedchem.0c01919
J. Med. Chem. 2021, 64, 1670−1684

282.2064; found, 282.2057; Anal. Calcd for $C_{16}H_{27}NO_3$: C, 68.29; H, 9.67; N, 4.98. Found: C, 68.33; H, 9.77; N, 4.97.

*Ethyl N,N-Diethyloxamate (**7b**).*[34] From 0.01 mol (0.73 g) of diethylamine (**6b**) in 20 mL of anhydrous THF, a yellow liquid was obtained (1.54 g, 89%); TLC (R_f = 0.92, petroleum ether and ethyl acetate, 1:1); ^{1}H NMR (300 MHz, $CDCl_3$, 25 °C): δ 4.34 (q, 2H, OCH_2CH_3, J = 7.0 Hz), 3.36, q, 4H, $N(CH_2CH_3)_2$, J = 7.3, 1.37, t, 3H, OCH_2CH_3, J = 7.0 Hz, 1.21, t, 6H, $N(CH_2CH_3)_2$, J = 7.3; ^{13}C NMR (75 MHz, $CDCl_3$, 25 °C): δ 163.2 (COO), 161.4 (CON), 61.8 (OCH_2CH_3), 42.4 (NCH_2CH_3), 39.0 (NCH_2CH_3), 14.1, 14.0, 12.5; HRMS (ESI/micrOTOF-Q) m/z: $[M + Na]^+$ calcd for $C_8H_{15}NO_3Na$, 196.0944; found, 196.0945: $[M + H]^+$ calcd for $C_8H_{16}NO_3$, 174.1125; found, 174.1123; Anal. Calcd for $C_8H_{15}NO_3$: C, 55.47; H, 8.73; N, 8.09. Found: C, 55.13; H, 8.40; N, 7.87.

*Hydrolysis of Esters **4a–e** and **7a–b**.* The esters (**4a–e** and **7a–b**) (0.001–0.003 mol) were saponified by dissolving them in 10 mL of THF and 5 mL of water and then adding 6 M aq KOH (2 mL). The resulting solution was heated under reflux for 1 h, maintaining the pH at 10, if needed, by the addition of additional 6 M KOH solution. After cooling to room temperature, the mixture was acidified to pH 3 by the addition of 10% aq HCl solution. The solvent was evaporated completely under reduced pressure, and the residue was extracted with EtOAc (3 × 10 mL). The organic layer was dried over anhydrous sodium sulfate, filtered, and evaporated again under reduced pressure to obtain the final hydroxyoxamate/oxamate compounds (**5a–e** and **8a–b**). No further purification was required.

*N-Cyclohexyl-N-hydroxyoxamate (**5a**).* From 0.003 mol (0.65 g) of compound **4a**, a brown solid was obtained (265 mg, 47%); mp 114.6–115.5 °C; ^{1}H NMR (300 MHz, DMSO-d_6, 25 °C): δ 10.11 (bs, N–O**H**, 1H), 3.91–4.01 (m, 1H, C_5H_{10}C**H**–**N**), 0.95–1.77 (m, 10H, C_5**H**$_{10}$CH–N); ^{13}C NMR (75 MHz, DMSO-d_6, 25 °C): δ 165.3 (COO), 162.4 (CON), 54.3 (C_5H_{10}CH), 28.9, 25.2, 25.1; HRMS (ESI/micrOTOF-Q) m/z: $[M - H]^-$ calcd for $C_8H_{12}NO_4$, 186.0772; found, 186.0773: $[M + Na - 2H]^-$ calcd for $C_8H_{11}NO_4Na$, 208.0591; found, 208.0591; Anal. Calcd for $C_8H_{13}NO_4$: C, 51.33; H, 7.00; N, 7.48. Found: C, 51.12; H, 7.01; N, 7.56.

*N-Cyclopentyl-N-hydroxyoxamate (**5b**).* From 0.002 mol (0.4 g) of compound **4b**, a brown solid was obtained (325 mg, 94%); mp 118.2–119.0 °C; ^{1}H NMR (300 MHz, DMSO-d_6, 25 °C): δ 10.10 (bs, 1H, N–O**H**), 4.53–4.63 (m, 1H, C_4H_8C**H**–**N**), 1.42–1.73 (m, 8H, C_4**H**$_8$CH–N); ^{13}C NMR (75 MHz, DMSO-d_6, 25 °C): δ 165.3 (COO), 162.7 (CON), 55.6 (C_4H_8CH), 28.3, 24.9; HRMS (ESI/micrOTOF-Q) m/z: $[M - H]^-$ calcd for $C_7H_{10}NO_4$, 172.0615; found, 172.0616: $[M + Na - 2H]^-$ calcd for $C_7H_9NO_4Na$, 194.0435; found, 194.0435; Anal. Calcd for $C_7H_{11}NO_4$: C, 48.55; H, 6.40; N, 8.09. Found: C, 48.54; H, 6.41; N, 8.41.

*N-(1-Phenylethyl)-N-hydroxyoxamate (**5c**).* From 0.001 mol (0.24 g) of compound **4c**, a brownish solid was obtained (950 mg, 45%); mp 105.2–106.0 °C; ^{1}H NMR (300 MHz, DMSO-d_6, 25 °C): δ 10.44 (bs, 1H, COO**H**), 7.23–7.44 (m, 5H, C_6**H**$_5$), 7.32 (bs, 1H, N–O**H**), 5.44 (q, 1H, C**H**CH_3, J = 6.0 Hz), 1.48 (d, 3H, $CHCH_3$, J = 6.0); ^{13}C NMR (75 MHz, DMSO-d_6, 25 °C): δ 165.2 (COO), 162.9 (CON), 140.5, 128.7, 127.8, 127.4, 53.7 ($CHCH_3$), 17.3 (CH_3); HRMS (ESI/micrOTOF-Q) m/z: $[M - H]^-$ calcd for $C_{10}H_{10}NO_4$, 208.0615; found, 208.0618: $[M + Na - 2H]^-$ calcd for $C_{10}H_9NO_4Na$, 230.0435; found, 230.0437; Anal. Calcd for $C_{10}H_{11}NO_4$: C, 57.41; H, 5.30; N, 6.70. Found: C, 57.19; H, 5.28; N, 6.42.

*N-Isobutyl-N-hydroxyoxamate (**5d**).* From 0.002 mol (0.38 g) of compound **4d**, an orange solid was obtained (166 mg, 51%); mp 75.3–77.0 °C; ^{1}H NMR (300 MHz, DMSO-d_6, 25 °C): δ 4.07–4.18 (m, 1H, CH_3CH_2C**H**CH_3), 1.34–1.46 (m, 2H, CH_3C**H**$_2CHCH_3$), 0.73–1.14 (m, 6H, C**H**$_3CH_2CHCH_3$); ^{13}C NMR (75 MHz, DMSO-d_6, 25 °C): δ 165.5 (COO), 163.2 (CON), 52.5 ($CH_3CH_2CHCH_3$), 25.9, 17.4, 11.1; HRMS (ESI/micrOTOF-Q) m/z: $[M - H]^-$ calcd for $C_6H_{10}NO_4$, 160.0615; found, 160.0615: $[M + Na - 2H]^-$ calcd for $C_6H_9NO_4Na$, 182.0435; found, 182.0437; Anal. Calcd for $C_6H_{11}NO_4$: C, 44.72; H, 6.88; N, 8.69. Found: C, 45.09; H, 7.23; N, 8.42.

*N-(4-Methyl-pent-2-yl)-N-hydroxyoxamate (**5e**).* From 0.002 mol (0.43 g) of compound **4e**, an orange liquid was obtained (197 mg, 52%); ^{1}H NMR (300 MHz, DMSO-d_6, 25 °C): δ 8.70 (bs, 1H, N–O**H**), 4.28–4.33, m, 1H, $(CH_3)_2CHCH_2$C**H**CH_3, 1.50–1.59, m, 2H, 1.07–1.17, m, 4H, 0.81–0.90, m, 6H; ^{13}C NMR (75 MHz, DMSO-d_6, 25 °C): δ 161.9 (COO), 157.3 (CON), 52.5 (N–C**H**CH_3), 42.1 $(CH_3)_2$C**H**$_2CHCH_3$, 24.5 $(CH_3)_2$C**H**$_2CHCH_3$, 23.5 and 21.9 $(CH_3)_2CHCH_2CHCH_3$, 18.2 $(CH_3)_2CHCH_2$C**H**CH_3; HRMS (ESI/micrOTOF-Q) m/z: $[M - H]^-$ calcd for $C_8H_{14}NO_4$, 188.0928; found, 188.0934: $[M + Na - 2H]^-$ calcd for $C_8H_{13}NO_4Na$, 210.0748; found, 210.0747.

*N,N-Dicyclohexyloxamate (**8a**).* From 0.001 mol (0.28 g) of compound **7a** in 10 mL of THF and 5 mL of water, a colorless solid was obtained (182 mg, 72%); mp 126.5–128.0 °C; ^{1}H NMR (300 MHz, DMSO-d_6, 25 °C): δ 3.04–3.21, m, 2H, 2(C_5H_{10}C**H**), 1.01–2.31, m, 20H, 2(C_5**H**$_{10}$CH); ^{13}C NMR (75 MHz, DMSO-d_6, 25 °C): δ 165.6 (COO), 163.3 (CON), 59.3 (C_5H_{10}CH), 54.5 (C_5H_{10}CH), 30.1, 29.6, 26.0, 25.7, 25.4, 24.8; HRMS (ESI/micrOTOF-Q) m/z: $[M - H]^-$ calcd for $C_{14}H_{22}NO_3$, 252.1605; found, 252.1612; Anal. Calcd for $C_{14}H_{23}NO_3$: C, 66.37; H, 9.15; N, 5.53. Found: C, 66.45; H, 9.23; N, 5.29.

*N,N-Diethyloxamate (**8b**).* From 0.003 mol (0.52 g) of compound **7b** in 10 mL of THF and 5 mL of water, a brown solid was obtained (133 mg, 31%); mp 90.0–91.2 °C; ^{1}H NMR (300 MHz, DMSO-d_6, 25 °C): δ 3.26, q, 4H, $N(CH_2CH_3)_2$, J = 7.3 Hz, 1.07, t, 6H, $N(CH_2CH_3)_2$, J = 7.3 Hz; ^{13}C NMR (75 MHz, DMSO-d_6, 25 °C): δ 165.6 (COO), 162.8 (CON), 42.2 (NCH_2CH_3), 38.2 (NCH_2CH_3), 14.5, 12.9; HRMS (ESI/micrOTOF-Q) m/z: $[M - H]^-$ calcd for $C_6H_{10}NO_3$, 144.0666; found, 144.0667; Anal. Calcd for $C_6H_{11}NO_3$: C, 49.65; H, 7.64; N, 9.65. Found: C, 49.67; H, 7.44; N, 9.51.

*Ethyl N-Benzyloxamate (**7c**).* To a vigorously stirring solution of benzylamine **6c** (0.03 mol, 3.22 g) in anhydrous THF (20 mL) at 5 °C was added a solution of EOC (0.01 mol, 1.37 g) in anhydrous THF (5 mL) dropwise during 15 min. The cooling bath was removed, and the mixture was stirred for 3 h under an atmosphere of nitrogen. The precipitated salt was filtered, and the solvent was evaporated under reduced pressure to give a white solid which was purified by flash chromatography, eluting with petroleum ether and ethyl acetate (7:3). Yield 65%, 1.34 g; mp 50.1–51.3 °C (lit.[35] mp 50–51 °C); TLC (R_f = 0.80, petroleum ether and ethyl acetate, 1:1); ^{1}H NMR (300 MHz, $CDCl_3$, 25 °C): δ 7.28–7.36 (m, 5H, C_6**H**$_5$), 4.53 (d, 2H, $C_6H_5CH_2$, J = 6.0 Hz), 4.36 (q, 2H, C**H**$_2CH_3$, J = 7.3 Hz), 1.40 (t, 3H, CH_2C**H**$_3$, J = 7.3 Hz); ^{13}C NMR (75 MHz, $CDCl_3$, 25 °C): δ 160.5 (COO), 156.4 (CON), 136.7 ($C_6H_5CCH_2$), 128.8, 128.0, 127.9, 63.3 (CH_2CH_3), 43.9 ($C_6H_5CCH_2$), 13.9 (CH_2CH_3); HRMS (ESI/micrOTOF-Q) m/z: $[M + Na]^+$ calcd for $C_{11}H_{13}NO_3Na$, 230.0788; found, 230.0782: $[M + H]^+$ calcd for $C_{11}H_{14}NO_3$, 208.0968; found, 208.0967; Anal. Calcd for $C_{11}H_{13}NO_3$: C, 63.76; H, 6.32; N, 6.76. Found: C, 63.84; H, 6.32; N, 6.87.

*N-Benzyloxamate (**8c**).* The ester **7c** was hydrolyzed using aq KOH and following the same procedure described in previous sections for the hydrolysis of esters.

From 0.002 mol (0.41 g) of compound **7c**, a colorless solid was obtained (160 mg, 45%); mp 117.0–119.0 °C (lit.[36] mp 118–120 °C); ^{1}H NMR (300 MHz, DMSO-d_6, 25 °C): δ 9.34 (t, 1H, J = 9.0 Hz), 7.20–7.34 (m, 5H), 4.31 (d, 2H, J = 9.0 Hz); ^{13}C NMR (75 MHz, DMSO-d_6, 25 °C): δ 162.6 (COO), 158.9 (CON), 139.0 ($C_6H_5CCH_2$), 128.7, 127.7, 127.4, 42.8 ($C_6H_5CCH_2$); HRMS (ESI/micrOTOF-Q) m/z: $[M - H]^-$ calcd for $C_9H_8NO_3$, 178.0510; found, 178.0510: $[M + Na - 2H]^-$ calcd for $C_9H_7NO_3Na$, 200.0329; found, 200.0331; Anal. Calcd for $C_9H_9NO_3$: C, 60.33; H, 5.06; N, 7.82. Found: C, 60.36; H, 5.15; N, 7.58.

*N-Isopropyloxamate (**8d**).*[37] EOC (0.010 mol, 1.38 g) was added dropwise to a solution of pyridine (0.01 mol, 0.8 g) and isopropylamine **6d** (0.030 mol, 1.8 g) in CH_2Cl_2 (20 mL) at 4 °C. The reaction mixture was stirred for 2 h at this temperature, allowed to warm to room temperature, and then washed with 1 M HCl (3 × 10 mL). The organic phase was shaken with 10 mL of 6 M aq KOH for 15 min. The aqueous phase was separated and acidified with 5 M HCl. Ether extraction and evaporation gave **8d** as a solid (473 mg, 36%); mp 107.5–108.7 °C (lit.[37] mp 110–113 °C); ^{1}H NMR (300 MHz, DMSO-d_6, 25 °C): δ 7.15 (bs, 1H, N**H**), 4.01–4.16 (m, 1H,

https://dx.doi.org/10.1021/acs.jmedchem.0c01919
J. Med. Chem. 2021, 64, 1670–1684

CH_3CHCH_3), 1.26 (d, 6H, CH_3CHCH_3, J = 6.0); ^{13}C NMR (75 MHz, DMSO-d_6): δ 162.8 (COO), 157.9 (CON), 41.5 (CH_3CHCH_3), 22.2 (CH_3); HRMS (ESI/micrOTOF-Q) m/z: $[M - H]^-$ calcd for $C_5H_8NO_3$, 130.0510; found, 130.0510: $[M + Na - 2H]^-$ calcd for $C_5H_7NO_3Na$, 152.0329; found, 152.0330; Anal. Calcd for $C_5H_9NO_3$: C, 45.80; H, 6.92; N, 10.68. Found: C, 46.15; H, 7.11; N, 10.97.

*N-Isobutyloxamate (**8e**).* This compound was prepared in an analogous manner to **8d**, except that isobutyamine was used in place of isopropylamine. From 0.005 mol of EOC in CH_2Cl_2 (20 mL), a colorless solid was obtained (710 mg, 49%); mp 104.4−105.3 °C (lit.[38] mp 106 °C); ^1H NMR (300 MHz, DMSO-d_6, 25 °C): δ 8.78 (bs, 1H, NH), 2.92, d, 2H, $(CH_3)_2CHCH_2$, J = 6.0, 1.70−1.83, m, 1H, $(CH_3)_2CHCH_2$, 0.82, d, 6H, $(CH_3)_2CHCH_2$, J = 6.0 Hz; ^{13}C NMR (75 MHz, DMSO-d_6, 25 °C): δ 162.8 (COO), 158.8 (CON), 46.8 $(CH_3)_2CHCH_2$, 28.2 $(CH_3)_2CHCH_2$, 20.4 $(CH_3)_2CHCH_2$; HRMS (ESI/micrOTOF-Q) m/z: $[M - H]^-$ calcd for $C_6H_{10}NO_3$, 144.0666; found, 144.0666: $[M + Na - 2H]^-$ calcd for $C_6H_9NO_3Na$, 166.0486; found, 166.0486; Anal. Calcd for $C_6H_{11}NO_3$: C, 49.65; H, 7.64; N, 9.65. Found: C, 49.70; H, 7.75; N, 9.77.

*N-(N-Boc-piperidin-4-yl)hydroxylamine (**10**).*[20] To a solution of *N*-Boc-piperidin-4-one (**9**) (0.04 mol, 8.0 g) in methanol (100 mL) was added acetic acid (0.07 mol, 4.2 g), sodium acetate (0.048 mol, 4.00 g), hydroxylamine hydrochloride (0.040 mol, 2.72 g), and sodium cyanoborohydride (0.12 mol, 7.68 g). The mixture was stirred overnight at room temperature. The solvent was removed under reduced pressure, and the residue was washed with saturated aqueous sodium bicarbonate solution. The aqueous layer was extracted with CH_2Cl_2 (3 × 100 mL). The combined organic phase was dried over anhydrous sodium sulfate, filtered, and evaporated under reduced pressure. The crude product was recrystallized from petroleum ether and chloroform (9:1) to give **10** as a cream solid (4.3 g, 50%); mp 117.2−118.4 °C; TLC R_f = 0.80, petroleum ether and ethyl acetate, 3:7. ^1H NMR (300 MHz, $CDCl_3$, 25 °C): δ 5.37 (bs, 2H, NHOH), 4.05−4.09 (m, 2H, HCH(N-Boc)HCH), 2.98−3.08 (m, 1H, $CH_2CH(NH-OH)CH_2$), 2.78−2.86 (m, 2H, HCH(N-Boc)HCH), 1.24−1.92 (m, 4H, $CH_2CH(NH-OH)CH_2$), 1.45, s, 9H, $(CH_3)_3CCOO$; ^{13}C NMR (75 MHz, $CDCl_3$, 25 °C): δ 154.7 $(CH_3)_3CCOO$, 79.6 $(CH_3)_3CCOO$, 58.7 (CHNHOH), 42.1 (CH_2NCH_2), 29.1 ($CH_2(CHNOH)CH_2$), 28.4 ($(CH_3)_3CCOO$).

*Ethyl N-Hydroxy-N-(N-Boc-piperidin-4-yl)oxamate (**11**).* To a solution of *N*-(*N*-Boc-piperidin-4-yl)hydroxylamine (**10**) (0.015 mol, 3.24 g) in THF (20 mL) at 4 °C under an atmosphere of nitrogen was added DIPEA (0.075 mol, 9.7 g) followed by the dropwise addition of EOC (0.030 mol, 4.1 g) during 15 min. The reaction mixture was allowed to warm to room temperature and stirred for 3 h, and then, the solvent was evaporated under reduced pressure. The residue was dissolved in petroleum ether and ethyl acetate (8:2), and the tertiary amine and its salt were removed by running the crude solution through a silica plug. The product was further purified by flash column chromatography, eluting with petroleum ether and ethyl acetate (1:1) to give **11** as a colorless solid (2.40 g, 51%); mp 141.8−142.5 °C; TLC (R_f = 0.54, petroleum ether and ethyl acetate, 1:1); ^1H NMR (300 MHz, $CDCl_3$, 25 °C): δ 8.16 (bs, 1H, NOH), 4.37 (q, 2H, CH_2CH_3, J = 7.0), 4.30−4.37 (m, 1H, CHNOH), 4.21 (bs, 2H), 2.71−2.88 (m, 2H), 1.71−2.13, m, 4H, $CH_2(CHNOH)CH_2$, 1.46, s, 9H, $(CH_3)_3CCOO$, 1.37−1.42, t, 3H, CH_2CH_3, J = 7.0; ^{13}C NMR (75 MHz, $CDCl_3$, 25 °C): δ 162.7 (COO), 161.0 (CON), 154.7 $(CH_3)_3CCOO$, 80.4 $(CH_3)_3CCOO$, 62.3 (CH_2CH_3), 57.7 (CHNOH), 42.8 (CH_2NCH_2), 29.1 ($CH_2(CHNOH)CH_2$), 28.4 ($(CH_3)_3CCOO$), 27.7 ($CH_2(CHNOH)CH_2$), 13.9 (CH_2CH_3); HRMS (ESI/micrOTOF-Q) m/z: $[M + Na]^+$ calcd for $C_{14}H_{24}N_2O_6Na$, 339.1527; found, 339.1529; Anal. Calcd for $C_{14}H_{24}N_2O_6$: C, 53.15; H, 7.65; N, 8.86. Found: C, 53.47; H, 7.68; N, 8.66.

*Ethyl N-Piperidin-4-yl-N-hydroxyoxamate Hydrochloride (**12**).* To a solution of ethyl *N*-hydroxy-*N*-(*N*-Boc-piperidin-4-yl)oxamate (**11**) (0.158 g, 0.50 mmol) in anhydrous THF (5 mL) was added 4 M dioxane-HCl (5 equiv). The reaction mixture was monitored by TLC and stirred at room temperature until the disappearance of the starting material (approximately 1 h). After the completion of the reaction, the solvent was evaporated completely under reduced pressure to give **12** as a white solid (yield 59%, 75 mg); mp 193.0−193.7 °C; ^1H NMR (300 MHz, D_2O, 25 °C): δ 4.33−4.50 (m, 1H, CHNOH), 4.26−4.34 (q, 2H, CH_2CH_3, J = 7.0 Hz), 3.02−3.50 (m, 4H, CH_2NHCH_2), 1.94−2.03, m, 4H, $CH_2(CHNOH)CH_2$, 1.21−1.26, t, 3H, CH_2CH_3, J = 7.0 Hz; ^{13}C NMR (75 MHz, D_2O): δ 163.1 (COO), 161.8 (CON), 63.8 (CH_2CH_3), 50.7 (CHNOH), 42.8 (CH_2NCH_2), 24.4 ($CH_2(CHNOH)CH_2$), 13.1 (CH_2CH_3); HRMS (ESI/micrOTOF-Q) m/z: $[M + H]^+$ calcd for $C_9H_{17}N_2O_4$, 217.1183; found, 217.1178; Anal. Calcd for $C_9H_{17}ClN_2O_4$: C, 42.78; H, 6.78; N, 11.09. Found: C, 42.59; H, 6.75; N, 10.78.

*Methyl N-Cyclopentyl-N-hydroxymalonate (**13**).* To a solution of the *N*-cyclopentylhydroxylamine (**3b**) (0.01 mol, 1.01 g) and DIPEA (0.01 mol, 1.29 g) in anhydrous THF (20 mL) at 4 °C was added methyl malonyl chloride (0.015 mol, 2.05 g) dropwise during 15 min under an atmosphere of nitrogen. The reaction mixture was allowed to warm to the room temperature and stirred for 3 h. The precipitated salt was filtered off, and the solvent was evaporated under reduced pressure to give crude methyl *N*-hydroxy-*N*-cyclopentylmalonate which was purified by flash chromatography, eluting with petroleum ether and ethyl acetate (3:7) to give **13** as a pale yellow liquid (0.40 g, 20%); TLC (R_f = 0.58, petroleum ether and ethyl acetate, 3:7); ^1H NMR (300 MHz, $CDCl_3$, 25 °C): δ 3.77 (s, 3H, CH_3), 3.61 (s, 2H, $COCH_2CO$), 3.50−3.57, m, 1H, $CH_2CH(NOH)CH_2$, 1.55−2.18, m, 8H, $CH_2CH_2CH_2CH_2$; ^{13}C NMR (75 MHz, $CDCl_3$): δ 170.5 (COO), 165.5 (CON), 56.5 ($CH_2CH(NOH)CH_2$), 52.8 (CH_3), 41.3 ($COCH_2CO$), 28.2, 24.8; HRMS (ESI/micrOTOF-Q) m/z: $[M + Na]^+$ calcd for $C_9H_{15}NO_4$, 224.0899; found, 224.0900; Anal. Calcd for $C_9H_{15}NO_4$: C, 53.72; H, 7.51; N, 6.96. Found: C, 53.71; H, 7.44; N, 6.64.

*N-Cyclopentyl-N-hydroxymalonate (**14**).* From 0.001 mol (0.20 g) of compound **13** in THF (10 mL), an orange liquid was obtained (yield 74%, 140 mg); ^1H NMR (300 MHz, DMSO-d_6, 25 °C): δ 9.59 (bs, 1H, NOH), 3.91 (s, 2H, $COCH_2CO$), 3.34−3.70, m, 1H, $CH_2CH(NOH)CH_2$, 1.43−1.69 (m, 8H, $CH_2CH_2CH_2CH_2$); ^{13}C NMR (75 MHz, DMSO-d_6): δ 169.0 (COO), 166.81 (CON), 55.5 ($CH_2CH(NOH)CH_2$), 40.9 ($COCH_2CO$), 28.0, 24.5; HRMS (ESI/micrOTOF-Q) m/z: $[M + Na]^+$ calcd for $C_8H_{13}NO_4Na$, 210.0742; found, 210.0731; Anal. Calcd for $C_8H_{13}NO_4$: C, 51.33; H, 7.00; N, 7.48. Found: C, 51.43; H, 7.04; N, 7.35.

*Preparation of n-Alkyl Esters (**23**−**27**) of **5b**.* The synthesis of compound **23** is described below as an example for this series of compounds.

(i) Monoesterification of oxalyl chloride

A solution of *n*-hexanol (63 μL, 51 mg, 0.5 mmol) in dry DCM (1 mL) was added dropwise to a solution of oxalyl chloride (0.25 mL, 370 mg, 2.9 mmol, 5.83 equiv) in dry DCM (2 mL) at 0 °C under a nitrogen atmosphere. The solution was stirred at room temperature for 14 h. The excess oxalyl chloride and solvent were removed by evaporation, and the oily product was used directly for the next step. (In the case of stearyl alcohol, the alcohol (333 μL, 271 mg, 1 mmol) was solubilized in dry DCM (1 mL) by warming the solution in a water bath at 50 °C. The dropping funnel was also heated gently using a heat gun to liquefy the dropping solution.)

(ii) Coupling of *N*-cyclopentylhydroxylamine (**3b**) with hexoxy oxalyl chloride

To a solution of the *N*-cyclopentylhydroxylamine (**3b**) (51 mg, 0.5 mmol) in anhydrous THF (3 mL), DIPEA (174 μL, 129 mg, 1 mmol, 2 equiv) was added. To this solution, hexoxy oxalyl chloride (96 mg, 0.5 mmol, 1 equiv) in anhydrous THF (2 mL) was added dropwise at 0 °C for 15 min under an atmosphere of nitrogen. After the addition, the ice bath was removed and the reaction mixture was allowed to warm to the room temperature and stirred for 14 h. The precipitated salt was filtered off using Celite as a filter aid, and the filtrate was evaporated under reduced pressure to get the desired ester compound hexyl *N*-hydroxy-*N*-cyclopentyloxamate (**23**) in the crude form as a brown oil which was further purified by flash chromatography using hexane and ethyl acetate (8:2).

https://dx.doi.org/10.1021/acs.jmedchem.0c01919
J. Med. Chem. 2021, 64, 1670−1684

*Hexyl N-Cyclopentyl-N-hydroxyoxamate (**23**).* From 0.5 mmol (51 mg) of *N*-cyclopentyl hydroxylamine (**3b**) in 3 mL of anhydrous THF, a brown oil was obtained (yield 58%, 75 mg); TLC (R_f = 0.38, hexane and ethyl acetate, 8:2); ^{1}H NMR (500 MHz, $CDCl_3$, 25 °C): δ 8.30 (bs, 1H, N−O**H**), 4.71 and 4.50 (2× quintet, 0.4H and 0.5H, C_4H_8C**H**−N, J = 7.2 and 7.5 Hz), 4.24 and 4.21 (2× t, 1.1H and 0.8H, CH_2CH_2O, J = 6.8 and 6.8 Hz), 1.98−1.65 (m, 8H, C_4H_8CH−N), 1.53−1.51 (m, 2H, C**H**$_2$CH$_2$O), 1.38−1.25 (m, 6H, $CH_3C_3H_6CH_2CH_2O$), 0.85 (t, 3H, C**H**$_3$CH$_2$, J = 7.0 Hz); ^{13}C NMR (125 MHz, $CDCl_3$, 25 °C): δ 163.9 (**C**OO), 160.7 (**C**ON), 154.5, 66.8, 66.4 (O**C**H$_2$), 60.7, 56.5 (C_4H_8**C**H), 31.24, 31.21, 29.3, 28.16, 28.11, 25.3, 25.2, 25.0, 24.7, 22.4, 13.9; HRMS (ESI/micrOTOF-Q) m/z: $[M + H]^+$ calcd for $C_{13}H_{24}NO_4^+$, 258.1700; found, 258.1701; and $[M + Na]^+$ calcd for $C_{13}H_{23}NNaO_4^+$, 280.1519; found, 280.1520; Anal. Calcd for $C_{13}H_{23}NO_4$: C, 60.68; H, 9.01; N, 5.44. Found: C, 60.40; H, 9.11; N, 5.15.

*Octyl N-Cyclopentyl-N-hydroxyoxamate (**24**).* From 0.5 mmol (51 mg) of *N*-cyclopentyl hydroxylamine (**3b**) in 3 mL of anhydrous THF, a brown oil was obtained (yield 31%, 88 mg); TLC (R_f = 0.31, hexane and ethyl acetate, 8:2); ^{1}H NMR (500 MHz, $CDCl_3$, 25 °C): δ 7.67 (bs, 1H, N−O**H**), 4.76 and 4.60 (2× quintet, 0.3H and 0.6H, C_4H_8C**H**−N, J = 7.1 and 7.0 Hz), 4.26 and 4.24 (t and m, 1.3H and 0.6H, CH_2CH_2O, J = 6.8), 2.00−1.68 (m, 8H, C_4H_8CH−N), 1.56−1.53 (m, 2H, C**H**$_2$CH$_2$O), 1.35−1.18 (m, 10H, $CH_3C_5H_{10}CH_2CH_2O$), 0.85 (t, 3H, C**H**$_3$CH$_2$, J = 6.9 Hz); ^{13}C NMR (125 MHz, $CDCl_3$, 25 °C): δ 163.7 (**C**OO), 160.5 (**C**ON), 160.3, 154.0, 66.9, 66.5 (O**C**H$_2$), 60.5, 56.6 (C_4H_8**C**H), 31.7, 29.4, 29.08, 29.07, 28.3, 28.2, 25.7, 25.6, 25.0, 24.7, 22.6, 14.0; HRMS (ESI/micrOTOF-Q) m/z: $[M + Na]^+$ calcd for $C_{15}H_{27}NNaO_4^+$, 308.1832; found, 308.1834; Anal. Calcd for $C_{15}H_{27}NO_4$: C, 63.13; H, 9.54; N, 4.91. Found: C, 62.72; H, 9.61; N, 5.21.

*Decyl N-Cyclopentyl-N-hydroxyoxamate (**25**).* From 0.5 mmol (51 mg) of *N*-cyclopentyl hydroxylamine (**3b**) in 3 mL of anhydrous THF, a brown oil was obtained (yield 41%, 64 mg); TLC (R_f = 0.48, hexane and ethyl acetate, 75:25); ^{1}H NMR (500 MHz, $CDCl_3$, 25 °C): δ 8.30 (bs, 1H, N−O**H**), 4.73 and 4.53 (2× quintet, 0.3H and 0.6H, C_4H_8C**H**−N, J = 7.5 and 7.5 Hz), 4.25 and 4.22 (2× t, 1.1H and 0.8H, CH_2CH_2O, J = 6.8 and 6.9 Hz), 2.00−1.65 (m, 8H, C_4H_8CH−N), 1.55−1.48 (m, 2H, C**H**$_2$CH$_2$O), 1.38−1.22 (m, 14H, $CH_3C_7H_{14}CH_2CH_2O$), 0.84 (t, 3H, C**H**$_3$CH$_2$, J = 7.0 Hz); ^{13}C NMR (125 MHz, $CDCl_3$, 25 °C): δ 163.9 (**C**OO), 160.65, 160.61 (**C**ON), 154.4, 66.9, 66.4 (O**C**H$_2$), 60.7, 56.5 (C_4H_8**C**H), 31.8, 29.44, 29.42, 29.40, 29.3, 29.2, 29.11, 29.08, 28.2, 28.1, 25.67, 25.60, 25.0, 24.7, 22.6, 14.0; HRMS (ESI/micrOTOF-Q) m/z: $[M + H]^+$ calcd for $C_{17}H_{32}NO_4^+$, 314.2326; found, 314.2319; and $[M + Na]^+$ calcd for $C_{17}H_{31}NNaO_4^+$, 336.2145; found, 336.2138; Anal. Calcd for $C_{17}H_{31}NO_4$: C, 65.14; H, 9.97; N, 4.47. Found: C, 64.87; H, 10.01; N, 4.30.

*Dodecyl N-Cyclopentyl-N-hydroxyoxamate (**26**).* From 0.5 mmol (51 mg) of *N*-cyclopentyl hydroxylamine (**3b**) in 3 mL of anhydrous THF, a brown oil was obtained (yield 44%, 75 mg); TLC (R_f = 0.51, hexane and ethyl acetate, 8:2); ^{1}H NMR (500 MHz, $CDCl_3$, 25 °C): δ 8.40 (bs, 1H, N−O**H**), 4.71 and 4.49 (2× quintet, 0.3H and 0.5H, C_4H_8C**H**−N, J = 7.3 and 7.5 Hz), 4.23 and 4.19 (2× t, 1.1H and 0.9H, CH_2CH_2O, J = 6.8 and 6.8 Hz), 1.99−1.62 (m, 8H, C_4H_8CH−N), 1.57−1.51 (m, 2H, C**H**$_2$CH$_2$O), 1.38−1.21 (m, 18H, $CH_3C_9H_{18}CH_2CH_2O$), 0.83 (t, 3H, C**H**$_3$CH$_2$, J = 7.0 Hz); ^{13}C NMR (125 MHz, $CDCl_3$, 25 °C): δ 163.8 (**C**OO), 160.74 (**C**ON), 160.69, 154.59, 66.8, 66.3 (O**C**H$_2$), 60.8, 56.5 (C_4H_8**C**H), 31.81, 31.80, 29.52, 29.50, 29.47, 29.44, 29.37, 29.25, 29.24, 29.08, 29.05, 28.2, 28.1, 25.63, 25.57, 25.0, 24.9, 24.7, 22.6, 14.0; HRMS (ESI/micrOTOF-Q) m/z: $[M + Na]^+$ calcd for $C_{19}H_{35}NNaO_4^+$, 364.2458; found, 364.2459; Anal. Calcd for $C_{19}H_{35}NO_4$: C, 66.83; H, 10.33; N, 4.10. Found: C, 66.95; H, 10.38; N, 4.23.

*Octadecyl N-Cyclopentyl-N-hydroxyoxamate (**27**).* From 1.0 mmol (101 mg) of *N*-cyclopentyl hydroxylamine (**3b**) in 5 mL of anhydrous THF, a brown oil was obtained (yield 21%, 91 mg); TLC (R_f = 0.27, hexane and ethyl acetate, 9:1); ^{1}H NMR (500 MHz, $CDCl_3$, 25 °C): δ 4.77 and 4.61 (2× quintet, 0.3H and 0.6H, C_4H_8C**H**−N, J = 7.2 and 7.5 Hz), 4.27 and 4.23 (2× t, 1.3H and 0.5H, CH_2CH_2O, J = 6.8 and 6.8 Hz), 2.02−1.67 (m, 8H, C_4H_8CH−N), 1.56−1.53 (m, 2H, C**H**$_2$CH$_2$O), 1.35−1.18 (m, 30H, $CH_3C_{15}H_{30}CH_2CH_2O$), 0.85 (t, 3H, C**H**$_3CH_2$, J = 7.0 Hz); ^{13}C NMR (125 MHz, $CDCl_3$, 25 °C): δ 163.7 (**C**OO), 160.5, 160.3 (**C**ON), 153.9, 66.9, 66.5 (O**C**H$_2$), 60.5, 56.6 (C_4H_8**C**H), 31.9, 29.7, 29.64, 29.61, 29.52, 29.45, 29.40, 29.3, 29.1, 28.3, 28.2, 25.72, 25.66, 25.1, 24.8, 22.7, 14.1; HRMS (ESI/micrOTOF-Q) m/z: $[M - H]^-$ calcd for $C_{25}H_{46}NO_4^-$, 424.3432; found, 424.3424; and $[M + Na]^+$ calcd for $C_{25}H_{47}NNaO_4^+$, 448.3397; found, 448.3393; Anal. Calcd for $C_{25}H_{35}NO_4$: C, 70.54; H, 11.13; N, 3.29. Found: C, 70.16; H, 11.07; N, 3.33.

Inhibition Assays. All analogues (100 μM) were incubated for 30 min with 0.27 μM *Mt*KARI in the assay buffer (50 μM NADPH, 50 mM Mg^{2+} and 0.1 M Tris−HCl, pH 8) at 25 °C. The reaction was initiated by the addition of 200 μM 2-acetolactate, and the decrease in absorbance at 340 nm was measured for 5 min. To determine the K_i of the compounds that showed more than 80% inhibition in this preliminary screening, the abovementioned assay was employed but with varying concentrations of inhibitors ranging from 1 nM to 100 μM. The K_i values of the most potent compounds were calculated by fitting the experimental data to the Morrison equation[15,22] using GraphPad Prism 6.0.[39]

Crystallization and Structure Determination of *Sa*KARI·Mg^{2+}·NADPH in Complex with 5a, 5b, and 5c. To prepare the samples for crystallization, 0.5 mM *Sa*KARI was incubated with 5 mM NADPH, 0.75 mM inhibitor, and 5 mM $MgCl_2$ for 30 min at room temperature. Crystals of *Sa*KARI·Mg^{2+}·NADPH in complex with **5b** were grown in a well solution containing 0.1 M imidazole (pH 8.0) and 17.5% PEG 8000, and crystals of *Sa*KARI·Mg^{2+}·NADPH in complex with **5a** and **5c** were grown in a well solution containing 0.2 M sodium acetate (pH 8.0) and 22.5% PEG 3350 by the hanging drop method. The plates were incubated at 16 °C for 7 days. Subsequently, the crystals were harvested and cryocooled using 20% glycerol as the cryoprotectant. The data were collected by remote access on beam line MX1 for **5b** and MX2 for **5a** and **5c** and processed using XDS.[40] Molecular replacement was performed using 5W3K (*Sa*KARI·Mg^{2+}·NADPH·CPD complex) as a template in Phenix[41] followed by model building using Coot 0.8.[42] The coordinates have been deposited in the Protein Data Bank with access codes 6C55 (**5a**), 6C5N (**5b**), and 6BUL (**5c**).

Molecular Docking. All of the designed compounds along with IpOHA were docked using the program Glide from Schrödinger.[43] A crystal structure of *Se*KARI·Mg^{2+}·NADPH·IpOHA (PDB code 4KQX) with identical active site residues to *Mt*KARI was used for docking. A protein file compatible for Glide docking was prepared by adding hydrogens. The entire protein was energy minimized using the OPLS 2005 force field. The search cube was limited to 8 Å in all directions with IpOHA at the center. All inhibitors were prepared for docking using the Ligprep module of the Schrödinger Maestro which produces different ionization states, and metal binding states were generated for pH 6.0−8.0 using the Epic module of Schrödinger Maestro. All possible stereoisomers were also generated, having different ionization states, stereoisomers, tautomers, and ring conformations. Flexible docking was performed by allowing the side-chain hydroxyl groups to rotate around the bond axis. Extra precision (XP)[43] docking was performed for all the molecules.

Resazurin Microtiter Assay. Compounds were tested using resazurin microtiter assay (REMA)[44] to calculate the minimum inhibitory concentration (MIC). Both virulent (H37Rv) and avirulent (H37Ra) strains of *Mt* were used. The bacteria were grown at 37 °C in defined minimal media (1 g of KH_2PO_4, 2.5 g of Na_2HPO_4, 0.5 g of L-asparagine, 5 mg of ferric ammonium citrate, 40 μM $MgSO_4$, 4.5 μM $CaCl_2$, 0.45 μM $ZnSO_4$, and 0.1% glycerol in 1 L H_2O) until the OD_{600} reached 0.4−0.8, which corresponds to the log/exponential phase. The culture was centrifuged at 800 rpm for 8 min to aggregate bacterial clumps and generated a single cell suspension. The OD of the bacterial suspension was measured, and necessary dilutions were made to reach the final OD of 0.001 for H37Ra and 0.003 for H37Rv. Serial dilutions (1:2) of the compounds with a starting concentration of 30 μM were performed in a 96-well plate. Rifampicin was used as

https://dx.doi.org/10.1021/acs.jmedchem.0c01919
J. Med. Chem. 2021, 64, 1670−1684

the control, and the plate was incubated at 37 °C for 5 days before adding resazurin. 24 h after the addition of resazurin, the fluorescence was measured with an excitation wavelength of 530 nm and emission wavelength at 590 nm. The data were analyzed, and inhibition curves were produced to obtain MIC_{90} using the Gompertz equation.[45]

Succinic Dehydrogenase (MTT) Assay. Three mammalian cells lines, RAW 264.7, HEK 293, and SW620, were grown to 80% confluency in DMEM (RAW 267.4 and HEK293) and RPMI (SW620) media with 10% fetal bovine serum and 1 mM nonessential amino acids and plated on 96-well plates at 2×10^5 RAW 264.7 cells, 5×10^3 HEK293 cells, and 2×10^3 SW620 cells, respectively, per well. The plates were incubated for 24−48 h at 37 °C and 5% CO_2. Twofold serial dilutions of **25** were prepared in 20% dimethyl sulfoxide (DMSO), and 10 μL of the compound was added to the wells to maintain 1% DMSO through the plate. The untreated cells and media-only controls were also added with 1% DMSO. The cells were incubated overnight at 37 °C and 5% CO_2. The MTT reagent (5 mg/mL) was added, and the plates were incubated for 3 h. The media was removed after 3 h, 50 μL of DMSO was added to the plates, and the contents were mixed by shaking the plates at 50 rpm for 2 min. Absorbance at 570 nm was measured, and data were plotted.

■ ASSOCIATED CONTENT

Supporting Information

The Supporting Information is available free of charge at https://pubs.acs.org/doi/10.1021/acs.jmedchem.0c01919.

Molecular formula strings (CSV)

Alignment of active site residues of *Mt* and *Sa*KARI; inhibition plots of compounds **4d**, **5a**, **5c**, and **5d** against *Mt*KARI; effects of hexanol, octanol, decanol, and dodecanol on the growth of H37Ra cells; and ^1H and ^{13}C NMR spectra of compounds **3e**, **4a−e**, **5a−e**, **7a−c**, **8a−e**, and **10−14** (PDF)

Compound 5a (PDB)

Compound 5b (PDB)

R isomer of compound 5c (PDB)

S isomer of compound 5c (PDB)

Accession Codes

Atomic coordinates have been deposited in the Protein Data Bank (https://rcsb.org) for *Sa*KARI in complex with **5a** (PDB ID: 6C5S), **5b** (PDB ID: 6C5N), and **5c** (PDB ID: 6BUL). The authors will release the atomic coordinates and experimental data upon article publication.

■ AUTHOR INFORMATION

Corresponding Author

Ross P. McGeary − *School of Chemistry and Molecular Biosciences, The University of Queensland, Brisbane, Queensland 4072, Australia;* orcid.org/0000-0001-9149-6264; Email: r.mcgeary@uq.edu.au

Authors

Ajit Kandale − *School of Chemistry and Molecular Biosciences, The University of Queensland, Brisbane, Queensland 4072, Australia*

Khushboo Patel − *School of Chemistry and Molecular Biosciences, The University of Queensland, Brisbane, Queensland 4072, Australia*

Waleed M. Hussein − *School of Chemistry and Molecular Biosciences, The University of Queensland, Brisbane, Queensland 4072, Australia*

Shun Jie Wun − *School of Chemistry and Molecular Biosciences, The University of Queensland, Brisbane, Queensland 4072, Australia*

Shan Zheng − *School of Chemistry and Molecular Biosciences, The University of Queensland, Brisbane, Queensland 4072, Australia*

Lendl Tan − *School of Chemistry and Molecular Biosciences, The University of Queensland, Brisbane, Queensland 4072, Australia;* orcid.org/0000-0002-9955-2440

Nicholas P. West − *School of Chemistry and Molecular Biosciences, The University of Queensland, Brisbane, Queensland 4072, Australia;* orcid.org/0000-0003-0955-9890

Gerhard Schenk − *School of Chemistry and Molecular Biosciences, The University of Queensland, Brisbane, Queensland 4072, Australia; Sustainable Minerals Institute and Australian Institute of Bioengineering and Nanotechnology, The University of Queensland, Brisbane, Queensland 4072, Australia*

Luke W. Guddat − *School of Chemistry and Molecular Biosciences, The University of Queensland, Brisbane, Queensland 4072, Australia;* orcid.org/0000-0002-8204-8408

Complete contact information is available at: https://pubs.acs.org/10.1021/acs.jmedchem.0c01919

Author Contributions

A.K. and K.P. are joint first authors. A.K. synthesized and characterized the compounds, other than the prodrugs; he also determined the K_i values of these compounds. A.K. performed docking, and K.P. grew the crystals and solved the crystal structures. W.M.H. synthesized and characterized the prodrug compounds. K.P., L.T., and S.J.W. performed the REMA assays, and W.M.H., S.J.W., and K.P. performed the MTT assays. S.J.W. purified the enzyme, and S.Z. helped in performing K_i assays. N.P.W., G.S., L.W.G., and R.P.M. were responsible for the experimental design and overall supervision of the project. All authors contributed to manuscript preparation.

Notes

The authors declare no competing financial interest.

■ ACKNOWLEDGMENTS

Initial crystallographic conditions were determined using the University of Queensland Remote-Operation Crystallization and X-ray Diffraction facility (UQROCX). X-ray measurements were performed at the Australian Synchrotron, ANSTO. This research was undertaken in part using the MX1 and MX2 beamline at the Australian Synchrotron and made use of the Australian Cancer Research Foundation (ACRF) detector. The work was funded by the National Health and Medical Research Foundation, grant number 114729. We thank Dr Thierry Lonhienne for helpful discussions, Dr Tri Le for assistance with NMR studies, and Dr Amanda Nouwens for mass spectrometry measurements.

■ ABBREVIATIONS

AHAS, acetohydroxyacid synthase; BCAA, branched-chain amino acids; DIPEA, *N*,*N*-diisopropylethylamine; DS, docking score; HOE 704, 2-(dimethylphosphoryl)-2-hydroxyacetic acid; IpOHA, *N*-hydroxy-*N*-isoproyloxamic acid; KARI, ketol-acid reductoisomerase; *Mt*, *Mycobacterium tuberculosis*; *Sa*, *Staphylococcus aureus*; *Se*, *Slackia exigua*

REFERENCES

(1) *Global Tuberculosis Report*, 2019. https://www.who.int/teams/global-tuberculosis-programme/tb-reports/global-report-2019 (accessed Nov 6, 2020).

(2) Rendon, A.; Tiberi, S.; Scardigli, A.; D'Ambrosio, L.; Centis, R.; Caminero, J. A.; Migliori, G. B. Classification of drugs to treat multidrug-resistant tuberculosis (MDR-TB): evidence and perspectives. *J. Thorac. Dis.* **2016**, *8*, 2666−2671.

(3) Singh, R.; Dwivedi, S. P.; Gaharwar, U. S.; Meena, R.; Rajamani, P.; Prasad, T. Recent updates on drug resistance in Mycobacterium tuberculosis. *J. Appl. Microbiol.* **2020**, *128*, 1547−1567.

(4) Grandoni, J. A.; Marta, P. T.; Schloss, J. V. Inhibitors of branched-chain amino acid biosynthesis as potential antituberculosis agents. *J. Antimicrob. Chemother.* **1998**, *42*, 475−482.

(5) Singh, B. K.; Shaner, D. L. Biosynthesis of branched-chain amino acids: from test tube to field. *Plant Cell* **1995**, *7*, 935−944.

(6) Leung, E. W. W.; Guddat, L. W. Conformational Changes in a Plant Ketol-Acid Reductoisomerase upon Mg2+ and NADPH Binding as Revealed by Two Crystal Structures. *J. Mol. Biol.* **2009**, *389*, 167−182.

(7) Tadrowski, S.; Pedroso, M. M.; Sieber, V.; Larrabee, J. A.; Guddat, L. W.; Schenk, G. Metal ions play an essential catalytic role in the mechanism of ketol−acid reductoisomerase. *Chem.—Eur. J.* **2016**, *22*, 7427−7436.

(8) Tyagi, R.; Lee, Y.-T.; Guddat, L. W.; Duggleby, R. G. Probing the mechanism of the bifunctional enzyme ketol-acid reductoisomerase by site-directed mutagenesis of the active site. *FEBS J.* **2005**, *272*, 593−602.

(9) Wong, S.-H.; Lonhienne, T. G. A.; Winzor, D. J.; Schenk, G.; Guddat, L. W. Bacterial and plant ketol-acid reductoisomerases have different mechanisms of induced fit during the catalytic cycle. *J. Mol. Biol.* **2012**, *424*, 168−179.

(10) Tyagi, R.; Duquerroy, S.; Navaza, J.; Guddat, L. W.; Duggleby, R. G. The crystal structure of a bacterial class II ketol-acid reductoisomerase: Domain conservation and evolution. *Protein Sci.* **2005**, *14*, 3089−3100.

(11) Garcia, M. D.; Nouwens, A.; Lonhienne, T. G.; Guddat, L. W. Comprehensive understanding of acetohydroxyacid synthase inhibition by different herbicide families. *Proc. Natl. Acad. Sci. U.S.A.* **2017**, *114*, E1091−E1100.

(12) Garcia, M. D.; Chua, S. M. H.; Low, Y.-S.; Lee, Y.-T.; Agnew-Francis, K.; Wang, J.-G.; Nouwens, A.; Lonhienne, T.; Williams, C. M.; Fraser, J. A.; Guddat, L. W. Commercial AHAS-inhibiting herbicides are promising drug leads for the treatment of human fungal pathogenic infections. *Proc. Natl. Acad. Sci. U.S.A.* **2018**, *115*, E9649−E9658.

(13) Liu, Y.; Bao, P.; Wang, D.; Li, Z.; Li, Y.; Tang, L.; Zhou, Y.; Zhao, W. Evaluation of the in vivo efficacy of novel monosubstituted sulfonylureas against H37Rv and extensively drug-resistant tuberculosis. *Jpn. J. Infect. Dis.* **2014**, *67*, 485−487.

(14) Aulabaugh, A.; Schloss, J. V. Oxalyl hydroxamates as reaction-intermediate analogs for ketol-acid reductoisomerase. *Biochemistry* **1990**, *29*, 2824−2830.

(15) Wun, S. J.; Johnson, L. A.; You, L.; McGeary, R. P.; Brueck, T.; Schenk, G.; Guddat, L. W. Inhibition studies of ketol-acid reductoisomerases from pathogenic microorganisms. *Arch. Biochem. Biophys.* **2020**, *692*, 108516.

(16) Lv, Y.; Kandale, A.; Wun, S. J.; McGeary, R. P.; Williams, S. J.; Kobe, B.; Sieber, V.; Schembri, M. A.; Schenk, G.; Guddat, L. W. Crystal structure of Mycobacterium tuberculosis ketol-acid reductoisomerase at 1.0 Å resolution - a potential target for anti-tuberculosis drug discovery. *FEBS J.* **2016**, *283*, 1184−1196.

(17) Patel, K. M.; Teran, D.; Zheng, S.; Kandale, A.; Garcia, M.; Lv, Y.; Schembri, M. A.; McGeary, R. P.; Schenk, G.; Guddat, L. W. Crystal Structures of Staphylococcus aureus Ketol-Acid Reductoisomerase in Complex with Two Transition State Analogues that Have Biocidal Activity. *Chem.—Eur. J.* **2017**, *23*, 18289−18295.

(18) Brinkmann-Chen, S.; Flock, T.; Cahn, J. K. B.; Snow, C. D.; Brustad, E. M.; McIntosh, J. A.; Meinhold, P.; Zhang, L.; Arnold, F. H. General approach to reversing ketol-acid reductoisomerase cofactor dependence from NADPH to NADH. *Proc. Natl. Acad. Sci. U.S.A.* **2013**, *110*, 10946−10951.

(19) Pirrung, M. C.; Han, H.; Ludwig, R. T. Inhibitors of Thermus thermophilus Isopropylmalate Dehydrogenase. *J. Org. Chem.* **1994**, *59*, 2430−2436.

(20) Garcia Rubio, S.; Pietra, C.; Giuliano, C.; Li, Z. Preparation of unsymmetric ureas as ghrelin receptor modulators and medical uses thereof. WO 2012113103 A1, 2012.

(21) Lee, Y.-T.; Ta, H. T.; Duggleby, R. G. Cyclopropane-1,1-dicarboxylate is a slow-, tight-binding inhibitor of rice ketol-acid reductoisomerase. *Plant Sci.* **2005**, *168*, 1035−1040.

(22) Morrison, J. F. The slow-binding and slow, tight-binding inhibition of enzyme-catalyzed reactions. *Trends Biochem. Sci.* **1982**, *7*, 102−105.

(23) Zhao, Q.; Cao, Y.; Wang, Y.; Hu, C.; Hu, A.; Ruan, L.; Bo, Q.; Liu, Q.; Chen, W.; Tao, F.; Ren, M.; Ge, Y.; Chen, A.; Li, L. Plasma and tissue free amino acid profiles and their concentration correlation in patients with lung cancer. *Asia Pac. J. Clin. Nutr.* **2014**, *23*, 429−436.

(24) Bayaraa, T.; Kurz, J. L.; Patel, K. M.; Hussein, W. M.; Bilyj, J. K.; West, N. P.; Schenk, G.; McGeary, R. P.; Guddat, L. W. Discovery, Synthesis and Evaluation of a Ketol-Acid Reductoisomerase Inhibitor. *Chem.—Eur. J.* **2020**, *26*, 8958−8968.

(25) Ngwerume, S.; Camp, J. E. Synthesis of Highly Substituted Pyrroles via Nucleophilic Catalysis. *J. Org. Chem.* **2010**, *75*, 6271−6274.

(26) Barber, G. N.; Olofson, R. A. A useful, regiospecific synthesis of isoxazoles. *J. Org. Chem.* **1978**, *43*, 3015−3021.

(27) Jain, N.; Kumar, A.; Chauhan, S. M. S. Metalloporphyrin and heteropoly acid catalyzed oxidation of CNOH bonds in an ionic liquid: biomimetic models of nitric oxide synthase. *Tetrahedron Lett.* **2005**, *46*, 2599−2602.

(28) Vavon, G.; Krajcinovic, N. Catalytic hydrogenation of oximes and their transformation into β-hydroxylamines. *Bull. Soc. Chim. Fr.* **1928**, *43*, 231−237.

(29) Borch, R. F.; Bernstein, M. D.; Durst, H. D. Cyanohydridoborate anion as a selective reducing agent. *J. Am. Chem. Soc.* **1971**, *93*, 2897−2904.

(30) Feuer, H.; Vincent, B. F., Jr. A convenient synthesis of N-alkylhydroxylamines. *J. Am. Chem. Soc.* **1962**, *84*, 3771−3772.

(31) Perrotti, E.; Daniele, M. L. G.; De Malde, M. Photochemical reactions of benzophenone. I. Reductions promoted by benzophenone-ketyl on monomer nitroso compounds and acyl radicals in photonitrosation and carbonylation of saturated hydrocarbons. *Ann. Chim.* **1965**, *55*, 485−493.

(32) Chang, Z. Y.; Coates, R. M. Diastereoselectivity of organometallic additions to nitrones bearing stereogenic N-substituents. *J. Org. Chem.* **1990**, *55*, 3464−3474.

(33) Geffken, D. Einfache und ergiebige Synthese substituierter N-Hydroxyoxamsäure-ester Facile and Efficient Synthesis of Esters of N-Substituted N-Hydroxyoxamic Acids. *Arch. Pharm.* **1987**, *320*, 382−384.

(34) Lynn, J. W.; English, J. Synthesis of Unsymmetrical α-Ketols by the Mixed Acyloin Reaction. *J. Am. Chem. Soc.* **1951**, *73*, 4284−4286.

(35) Lambert, J. B.; Huseland, D. E.; Wang, G.-t. Synthesis of 1,3-disubstituted diazolidines. *Synthesis* **1986**, *1986*, 657−658.

(36) Mecinovic, J.; Loenarz, C.; Chowdhury, R.; Schofield, C. J. 2-Oxoglutarate analogue inhibitors of prolyl hydroxylase domain 2. *Bioorg. Med. Chem. Lett.* **2009**, *19*, 6192−6195.

(37) Pirrung, M. C.; Han, H.; Ludwig, R. T. Inhibitors of Thermus thermophilus Isopropylmalate Dehydrogenase. *J. Org. Chem.* **1994**, *59*, 2430−2436.

(38) Jacobson, M. Pellitorine Isomers. II. The Synthesis of N-Isobutyl-trans-2,trans-4-decadienamide1,2,3. *J. Am. Chem. Soc.* **1953**, *75*, 2584−2586.

(39) *Graphpad Prism 6.0*; G. S., Inc: CA, USA, 2014.

(40) Kabsch, W. XDS. *Acta Crystallogr., Sect. D: Biol. Crystallogr.* **2010**, *66*, 125−132.

https://dx.doi.org/10.1021/acs.jmedchem.0c01919
J. Med. Chem. 2021, 64, 1670−1684

(41) Adams, P. D.; Afonine, P. V.; Bunkóczi, G.; Chen, V. B.; Davis, I. W.; Echols, N.; Headd, J. J.; Hung, L.-W.; Kapral, G. J.; Grosse-Kunstleve, R. W.; McCoy, A. J.; Moriarty, N. W.; Oeffner, R.; Read, R. J.; Richardson, D. C.; Richardson, J. S.; Terwilliger, T. C.; Zwart, P. H. PHENIX: a comprehensive Python-based system for macromolecular structure solution. *Acta Crystallogr., Sect. D: Biol. Crystallogr.* **2010**, *66*, 213−221.
(42) Emsley, P.; Lohkamp, B.; Scott, W. G.; Cowtan, K. Features and development of Coot. *Acta Crystallogr., Sect. D: Biol. Crystallogr.* **2010**, *66*, 486−501.
(43) Friesner, R. A.; Murphy, R. B.; Repasky, M. P.; Frye, L. L.; Greenwood, J. R.; Halgren, T. A.; Sanschagrin, P. C.; Mainz, D. T. Extra Precision Glide: Docking and Scoring Incorporating a Model of Hydrophobic Enclosure for Protein-Ligand Complexes. *J. Med. Chem.* **2006**, *49*, 6177−6196.
(44) Palomino, J.-C.; Martin, A.; Camacho, M.; Guerra, H.; Swings, J.; Portaels, F. Resazurin microtiter assay plate: simple and inexpensive method for detection of drug resistance in Mycobacterium tuberculosis. *Antimicrob. Agents Chemother.* **2002**, *46*, 2720−2722.
(45) Lambert, R. J. W.; Pearson, J. Susceptibility testing: accurate and reproducible minimum inhibitory concentration (MIC) and non-inhibitory concentration (NIC) values. *J. Appl. Microbiol.* **2000**, *88*, 784−790.

https://dx.doi.org/10.1021/acs.jmedchem.0c01919
J. Med. Chem. 2021, 64, 1670−1684